

A Multiscale Discontinuous Galerkin Method with the Computational Structure of a Continuous Galerkin Method

Thomas J.R. Hughes

Institute for Computational Engineering and Sciences
The University of Texas at Austin, Austin, USA

Guglielmo Scovazzi

9231 Computational Physics R&D Department,
Sandia National Laboratories, Albuquerque, New Mexico, USA

Pavel B. Bochev

9214 Computational Mathematics and Algorithms Department,
Sandia National Laboratories, Albuquerque, New Mexico, USA

Annalisa Buffa

IMATI - Consiglio Nazionale delle Ricerche, Pavia, Italy

June 28, 2005

Abstract

Proliferation of degrees-of-freedom has plagued discontinuous Galerkin methodology from its inception over thirty years ago. This paper develops a new computational formulation that combines the advantages of discontinuous Galerkin methods with the data structure of their continuous Galerkin counterparts. The new method uses local, element-wise problems to project a continuous finite element space into a given discontinuous space, and then applies a discontinuous Galerkin formulation. The projection leads to parameterization of the discontinuous degrees-of-freedom by their continuous counterparts and has a variational multiscale interpretation. This significantly reduces the computational burden and, at the same time, little or no degradation of the solution occurs. In fact, the new method produces improved solutions compared with the traditional discontinuous Galerkin method in some situations.

Contents

1 Introduction

2

2	Advection-Diffusion Equation	3
2.1	Strong form of the problem	4
2.2	Definitions and notations for the discontinuous Galerkin method	4
3	Global Weak Formulation	7
3.1	Conservative formulation	7
3.1.1	Conservation properties	8
3.1.2	Euler-Lagrange equations	9
4	Local Weak Formulations	10
4.1	Local problem for the trial solution	10
4.1.1	Multiscale interpretation	12
4.2	Local problem for the weighting function	13
5	Numerical Results	14
5.1	One-dimensional advection-diffusion	14
5.1.1	Weak formulation	14
5.1.2	Local problem for the trial solution	14
5.1.3	Limit behavior	16
5.1.4	Local problem for the weighting function	17
5.1.5	Numerical results	17
5.2	Two-dimensional advection equation	27
5.2.1	Advection skew to the mesh	27
5.2.2	Rotating flow	28
6	Conclusions and Future Directions	32

1 Introduction

The discontinuous Galerkin (DG) method was developed for problems of neutron transport over thirty years ago by Reed and Hill [46]. Early works of note include Lesaint and Raviart [42], Johnson, Nävert and Pitkäranta [40] who, in the context of advection-dominated processes, synthesized DG with SUPG [10] and performed a complete mathematical analysis, and Johnson and Pitkäranta [41], who proved that the DG formulation for pure advection problems enjoys good stability properties, similar to the ones proved for SUPG. The interest in DG developed very slowly but has accelerated significantly in recent years. The compendium of papers in [13] provides a valuable summary of the current state-of-the-art and introduction to the literature. Recent literature on DG methods includes [1, 2, 5, 12, 15–18, 25, 27–30, 43–45, 49, 50].

The DG method is felt to have advantages of robustness over the classical continuous Galerkin (CG) method, especially for first-order differential operators associated with hyperbolic equations, and better conditioning of resultant linear equation systems leading to improved iterative performance. There is also an opportunity to link DG with the numerical fluxes (i.e., solutions of the one-dimensional Riemann problem) used in finite volume methods and develop higher-order accurate procedures for wave-propagation. These attributes have led to numerous applications in fluids where the CG method has often proved inadequate. There has also been recent interest in applying DG to elliptic problems so that advective-diffusive phenomena can be modeled. For a review of work in this area, see Arnold *et al.* [3]. Recent studies include Brezzi *et al.* [7], Dawson [14], and Hughes, Masud and Wan [37]. There has been very little work in structural

mechanics so far but interest is beginning to grow. See for example, Engel *et al.*[23], and Brezzi and Marini [8].

Despite the increased interest in DG methods, there are shortcomings that limit their practical utility. Foremost among these is the size of the DG equation system for interpolations of linear and higher order. By virtue of the fact that the trial functions are completely discontinuous, there is no sharing of degrees-of-freedom at element boundaries. Consequently, the size of the solution space “explodes.” For example, assuming about seven linear tetrahedral elements per node, the DG system involves approximately 28 times the number of unknowns of the corresponding CG system (see Hughes *et al.* [32]). Storage and solution cost are, obviously, adversely affected, which seems the main reason for the small industrial impact the DG method has had so far. In addition, it has been observed that the vaunted robustness of the DG method is somewhat exaggerated. Simple, one-dimensional examples of pure advection and pure diffusion were shown to give rise to spurious oscillations in Hughes *et al.* [32].

There are two perspectives on the proposed new method. One is to assume a given, continuous finite element space, and then associate to it a completely discontinuous space by releasing all continuity constraints at element interfaces. This viewpoint is somewhat restrictive but is applicable to most situations of engineering interest and therefore is adopted in this paper. Another, more general, view is to start with an arbitrary discontinuous finite element space and then construct a continuous representation from it. This viewpoint will be developed in a forthcoming work of the authors. Once the spaces are defined, a global DG formulation is applied to the discontinuous space. The unique feature of our formulation is the use of local, element-wise problems, to define the discontinuous field in terms of the degrees-of-freedom of the continuous field. The local problems employ weakly imposed boundary conditions and the solutions are still discontinuous but they are parameterized by the degrees-of-freedom of the much smaller continuous space. The global problem has the equation size and structure of a CG method but it is indeed a DG method. The local problems serve to project the solution into a reduced-dimension manifold that expresses the partial-differential structure of the problem considered. This aspect is seen to be related to methods used in wave propagation problems, relying on numerical fluxes inspired by local Riemann solutions, but here the local problems are solved numerically using simple basis functions. The interesting result is that the new method is at least as accurate and robust as the global DG method, and, at the same time, the storage and computational effort are dramatically reduced. As may be obvious from the description, the method has a multiscale interpretation. For this reason, we refer to it as the multiscale DG method (MDG).

The new method is demonstrated on simple test cases of advection-diffusion. However, the ideas are quite general and may be applied to arbitrary partial-differential equation systems. Section 2 is devoted to the introduction of the advection-diffusion problem, to prepare the ground for the global DG formulation presented in Section 3. Three variants of the discretization of the Laplace operator are considered: the symmetric, neutral, and skew-symmetric forms. The local problem is described in Section 4. The weak formulation is similar to the one used for the global problem, but an additional stabilization term is required. Numerical results are presented in Section 5, and conclusions are drawn in Section 6.

2 Advection-Diffusion Equation

This section describes the boundary-value problem for the linear advection-diffusion equation and introduces definitions and notations needed for the DG formulation presented subsequently.

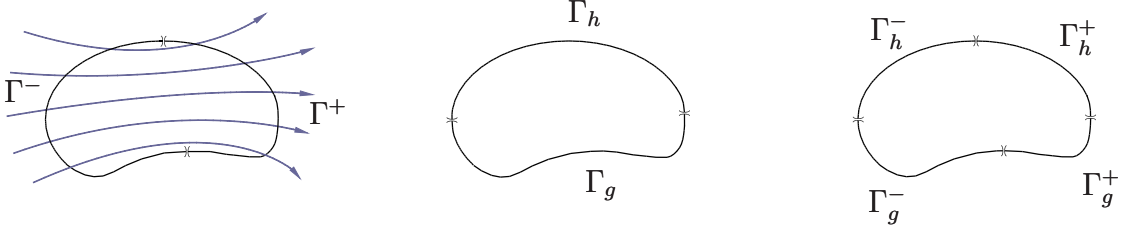


Figure 1: Boundary partitions.

2.1 Strong form of the problem

Let Ω be a bounded domain in \mathbb{R}^{n_d} , where n_d is the number of space dimensions, let \mathbf{a} be a smooth, solenoidal, velocity vector field defined on $\overline{\Omega}$, and let κ be a positive, constant, diffusivity coefficient. Consider the following partition of the boundary $\Gamma = \partial\Omega$:

$$\Gamma^- = \{x \in \Gamma : \mathbf{a}(x) \cdot \mathbf{n}(x) \leq 0\} \quad (1)$$

$$\Gamma^+ = \{x \in \Gamma : \mathbf{a}(x) \cdot \mathbf{n}(x) > 0\} \quad (2)$$

where \mathbf{n} is the outward unit normal with respect to Γ . Γ^- is referred to as the inflow boundary and Γ^+ as the outflow boundary. Another partition is given by $\Gamma = \overline{\Gamma_h \cup \Gamma_g}$, $\Gamma_h \cap \Gamma_g = \emptyset$, and thus

$$\Gamma_g^\mp = \Gamma_g \cap \Gamma^\mp \quad (3)$$

$$\Gamma_h^\mp = \Gamma_h \cap \Gamma^\mp \quad (4)$$

The setup is illustrated in Figure 1. The strong form of the boundary-value problem is:

Find $\phi : \overline{\Omega} \rightarrow \mathbb{R}$, such that for all $f : \Omega \rightarrow \mathbb{R}$, $g : \Gamma \rightarrow \mathbb{R}$, and $h : \Gamma \rightarrow \mathbb{R}$,

$$\mathbf{a} \cdot \nabla \phi - \kappa \Delta \phi = f \quad \text{in } \Omega \quad (5)$$

$$\phi = g \quad \text{on } \Gamma_g \quad (6)$$

$$(-\mathbf{a}\phi\chi_{\Gamma_h^-} + \kappa\nabla\phi) \cdot \mathbf{n} = h \quad \text{on } \Gamma_h \quad (7)$$

where $\chi_{\Gamma_h^-}$ is the characteristic function of the set Γ_h^- . The meaning of the boundary condition on Γ_h is that the total flux (advective plus diffusive) is imposed on the boundary Γ_h^- and the diffusive flux is specified on the boundary Γ_h^+ . For further insight into these boundary conditions, see Hughes, Franca and Hulbert [34].

2.2 Definitions and notations for the discontinuous Galerkin method

Let \mathcal{T}_h be a regular family of elements T generating a partition of Ω . For example, T can be thought of as triangles/tetrahedra, or quadrilaterals/hexahedra, in two/three dimensions, respectively. Let h_T denote the diameter of T and $h = \max_{T \in \mathcal{T}_h} h_T$. Let \mathcal{E}_h be the set of element edges (including edges on the boundary Γ) and \mathcal{E}_h^o be the set of internal edges (excluding edges on the boundary Γ). It follows that

$$\mathcal{E}_h = \mathcal{E}_h^o \cup \Gamma \quad (8)$$

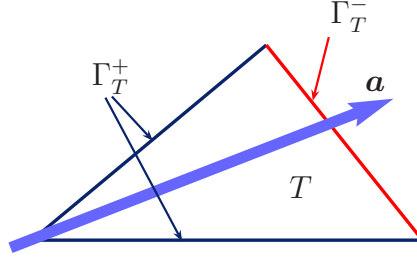


Figure 2: Schematic of the inflow and outflow boundaries for an element with respect to the convective field \mathbf{a} .

It is also helpful to define inflow and outflow partitions of the element boundary $\Gamma_T = \partial T$ (see Fig. 2):

$$\Gamma_T^- = \{x \in \Gamma_T : \mathbf{a}(x) \cdot \mathbf{n}(x) \leq 0\} \quad (9)$$

$$\Gamma_T^+ = \{x \in \Gamma_T : \mathbf{a}(x) \cdot \mathbf{n}(x) > 0\} \quad (10)$$

In order to derive a DG formulation, jumps and averages of scalar and vector functions have to be defined on \mathcal{E}_h . We shall employ the Brezzi conventions for this purpose. For an interior edge $e \in \mathcal{E}_h^o$, let T^+ and T^- be the two elements sharing it, and let \mathbf{n}^+ and \mathbf{n}^- be their respective outward-pointing unit normals (see Fig. 3). Accordingly, let φ be a scalar field, and $\varphi^\pm := \varphi|_{T^\pm}$. For $e \in \mathcal{E}_h^o$:

$$\langle \varphi \rangle := \frac{1}{2}(\varphi^+ + \varphi^-) \quad (11)$$

$$\llbracket \varphi \rrbracket := \varphi^+ \mathbf{n}^+ + \varphi^- \mathbf{n}^- \quad (12)$$

Analogously, if $\boldsymbol{\tau}$ is a vector field,

$$\langle \boldsymbol{\tau} \rangle := \frac{1}{2}(\boldsymbol{\tau}^+ + \boldsymbol{\tau}^-) \quad (13)$$

$$\llbracket \boldsymbol{\tau} \rrbracket := \boldsymbol{\tau}^+ \cdot \mathbf{n}^+ + \boldsymbol{\tau}^- \cdot \mathbf{n}^- \quad (14)$$

Notice that, by definition of “ $\llbracket \cdot \rrbracket$ ”, the jump of a scalar quantity is a vector and the jump of a vector quantity is a scalar. Definitions (12) and (14) do not depend on the ordering of the elements. It is important to specialize the previous formulas to the edges on the boundary Γ :

$$\llbracket \varphi \rrbracket = \varphi \mathbf{n}, \quad \langle \boldsymbol{\tau} \rangle = \boldsymbol{\tau}, \quad \forall e \in \Gamma \quad (15)$$

It will not be necessary to define $\langle \varphi \rangle$ and $\llbracket \boldsymbol{\tau} \rrbracket$ on the boundary Γ , because they are never utilized. Noting that

$$\begin{aligned} \llbracket \varphi \boldsymbol{\tau} \rrbracket &= \varphi^+ \boldsymbol{\tau}^+ \cdot \mathbf{n}^+ + \varphi^- \boldsymbol{\tau}^- \cdot \mathbf{n}^- \\ &= \frac{1}{2} (2\varphi^+ \boldsymbol{\tau}^+ \cdot \mathbf{n}^+ + 2\varphi^- \boldsymbol{\tau}^- \cdot \mathbf{n}^-) \\ &= \frac{\varphi^+ + \varphi^-}{2} (\boldsymbol{\tau}^+ \cdot \mathbf{n}^+ + \boldsymbol{\tau}^- \cdot \mathbf{n}^-) + \frac{\boldsymbol{\tau}^+ + \boldsymbol{\tau}^-}{2} \cdot (\varphi^+ \mathbf{n}^+ + \varphi^- \mathbf{n}^-) \\ &= \langle \varphi \rangle \llbracket \boldsymbol{\tau} \rrbracket + \langle \boldsymbol{\tau} \rangle \cdot \llbracket \varphi \rrbracket \end{aligned} \quad (16)$$

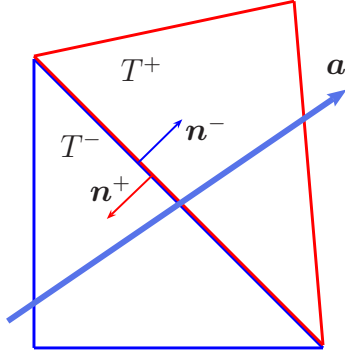


Figure 3: Schematic of the normals and $+/-$ regions with respect to an edge.

and accounting for (15), it follows that

$$\sum_{T \in \mathcal{T}_h} \int_{\partial T} \boldsymbol{\tau} \cdot \mathbf{n} \varphi = \sum_{e \in \mathcal{E}_h} \int_e \langle \boldsymbol{\tau} \rangle \cdot \llbracket \varphi \rrbracket + \sum_{e \in \mathcal{E}_h^o} \int_e \llbracket \boldsymbol{\tau} \rrbracket \langle \varphi \rangle \quad (17)$$

Another important identity is

$$\begin{aligned} \llbracket \varphi \boldsymbol{\tau} \rrbracket &= \varphi^+ \boldsymbol{\tau}^+ \cdot \mathbf{n}^+ + \varphi^- \boldsymbol{\tau}^- \cdot \mathbf{n}^- \\ &= \varphi^+ \boldsymbol{\tau}^+ \cdot \mathbf{n}^+ + \varphi^\pm \boldsymbol{\tau}^\mp \cdot \mathbf{n}^- + \varphi^\pm \boldsymbol{\tau}^\mp \cdot \mathbf{n}^+ + \varphi^- \boldsymbol{\tau}^- \cdot \mathbf{n}^- \\ &= \varphi^\pm \llbracket \boldsymbol{\tau} \rrbracket + \llbracket \varphi \rrbracket \cdot \boldsymbol{\tau}^\mp \end{aligned} \quad (18)$$

which implies

$$\sum_{T \in \mathcal{T}_h} \int_{\partial T} \boldsymbol{\tau} \cdot \mathbf{n} \varphi = \sum_{e \in \mathcal{E}_h} \left(\int_e \varphi^\pm \llbracket \boldsymbol{\tau} \rrbracket + \int_e \llbracket \varphi \rrbracket \cdot \boldsymbol{\tau}^\mp \right) + \sum_{e \in \Gamma} \int_e \varphi \boldsymbol{\tau} \cdot \mathbf{n} \quad (19)$$

This last result will be used in the sequel to recover the Euler-Lagrange forms of variational problems.

Following the perspective on the new method adopted in Section 1 we first introduce the *continuous* finite element space

$$\overline{V}_h^k = \{v \in H^1(\Omega) : v|_T \in \mathcal{P}^k(T), \quad \forall T \in \mathcal{T}_h\} \quad (20)$$

where \mathcal{P}^k is the space of polynomials of degree less than or equal to k , and then associate with it the *discontinuous* approximation space

$$V_h^k = \{v \in L^2(\Omega) : v|_T \in \mathcal{P}^k(T), \quad \forall T \in \mathcal{T}_h\}. \quad (21)$$

According to the interpretation in Section 1 we will view V_h^k as being obtained from \overline{V}_h^k by releasing interelement continuity constraints.

3 Global Weak Formulation

In this section a global DG method is presented which will serve as a framework for the solution of the advection-diffusion problem. Skew-symmetric, neutral, and symmetric versions of the DG method are considered. They will be integrated into the global formulation by introducing a switch s , taking the values $+1$, 0 , and -1 , respectively. The symmetric version is the only one which yields a symmetric discretization of the Laplace operator and is the only one that is adjoint consistent, following the terminology of Arnold *et al.* [3].

3.1 Conservative formulation

One of the most important design requirements for DG formulations is conservation. In the present formulation a new approach is taken to enforce conservation of the total flux $\sigma := \mathbf{a}\phi_h - \kappa\nabla\phi_h$. The global DG formulation reads:

$$\begin{aligned}
& \text{Find } \phi_h \in V_h^k \text{ such that, } \forall \mu_h \in V_h^k, \\
0 &= \sum_{T \in \mathcal{T}_h} \left(- \int_T \nabla \mu_h \cdot (\mathbf{a}\phi_h - \kappa\nabla\phi_h) - \int_T \mu_h f \right) \\
&+ \sum_{e \in \Gamma_g} \left(\int_e \mu_h (\mathbf{a}(\chi_{\Gamma_g^-} g + \chi_{\Gamma_g^+} \phi_h) - \kappa\nabla\phi_h) \cdot \mathbf{n} + \int_e \left(\frac{\epsilon\kappa}{h_\perp} \mu_h + s\kappa\nabla\mu_h \cdot \mathbf{n} \right) (\phi_h - g) \right) \\
&+ \sum_{e \in \Gamma_h} \int_e \mu_h \left((\mathbf{a}\phi_h) \chi_{\Gamma_h^+} \cdot \mathbf{n} - h \right) \\
&+ \sum_{e \in \mathcal{E}_h^o} \left(\int_e ([\mu_h] \cdot (\mathbf{a}\phi_h^- - \kappa\nabla\phi_h^-) + s\kappa\nabla\mu_h^- \cdot [\phi_h]) + \int_e \frac{\epsilon\kappa}{h_\perp} [[\mu_h]] \cdot [[\phi_h]] \right) \tag{22}
\end{aligned}$$

The following definition will be used:

$$h_\perp = \frac{\text{meas}(T^+) + \text{meas}(T^-)}{2 \text{meas}(e)} \tag{23}$$

where T^-/T^+ are, respectively, the upwind/downwind elements with respect to the edge e . Roughly speaking, h_\perp is a length scale in the direction perpendicular to the edge e , close to the length of the segment joining the barycenters of T^- and T^+ (see Fig. 4). The selection of the value of the non-dimensional parameter ϵ will be described subsequently.

Remark

The effect of the parameter s has been extensively studied in the discontinuous Galerkin literature (see Arnold *et al.* [3], Baumann and Oden [4], and Hughes *et al.* [32]). The symmetric formulation (i.e., $s = -1$) is adjoint-consistent, guaranteeing optimal L_2 -convergence rates in the diffusive limit. Ostensibly, the skew formulation (i.e., $s = +1$) has superior stability properties but the ϵ -terms can be used to improve the stability behavior of the neutral (i.e., $s = 0$) and symmetric formulations.

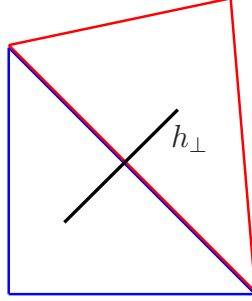


Figure 4: Definition of h_\perp for two adjacent triangular elements.

3.1.1 Conservation properties

In many applications global and/or local conservation is important. Our DG formulation (22) possesses exactly the same global conservation as a continuous Galerkin method. To extract a statement of conservation, consider the case $\Gamma_g = \emptyset$ and set the weighting function μ_h in (22) equal to one throughout Ω . It is easily seen that the finite element solution ϕ_h satisfies

$$\int_{\Omega} f + \int_{\Gamma_{h^-}} h^- + \int_{\Gamma_{h^+}} (-\mathbf{a} \cdot \mathbf{n} \phi_h + h^+) = 0. \quad (24)$$

which is identical with the conservation statement of a standard Galerkin method; see [39].

To extract a local conservation statement, consider for simplicity an element T that does not have edges on the boundary Γ and a weight function μ_h that equals one on T and zero on all other elements. Then, (22) reduces to

$$-\int_T f + \sum_{e \in \partial T} \left(\int_e (\mathbf{a} \phi_h^- - \kappa \nabla \phi_h^-) \cdot \mathbf{n} + \int_e \frac{\varepsilon \kappa}{h_\perp} \llbracket \phi_h \rrbracket \cdot \mathbf{n} \right) = 0, \quad (25)$$

where we have used that for the given choice of μ_h the jump $\llbracket \mu_h \rrbracket$ is simply the outer normal \mathbf{n} to ∂T . Without the stabilization term (25) specializes to

$$-\int_T f + \sum_{e \in \partial T} \int_e (\mathbf{a} \phi_h^- - \kappa \nabla \phi_h^-) \cdot \mathbf{n} = 0, \quad (26)$$

i.e., the DG method (22) is locally conservative. When $\varepsilon > 0$ local conservation is exact to order $O(\varepsilon)$. This situation is typical of all DG methods that employ interior penalty terms for stabilization. Then the strong local conservation is weakened in the sense that the element conservation law involves terms from *all* surrounding elements, contributed by the last term in (25). This is reminiscent of what occurs in CG methods, the ε -terms here enforcing a weak continuity. It should be noted however, that local conservation is a topological property, while stability and convergence are metric properties, and so, the weakened local conservation does not imply inferior convergence or stability of the DG scheme.

As a final note, we point out that in most DG formulations advective fluxes are *upwinded* while diffusive fluxes are *centered*. This leads to conservation of fluxes that are not located at

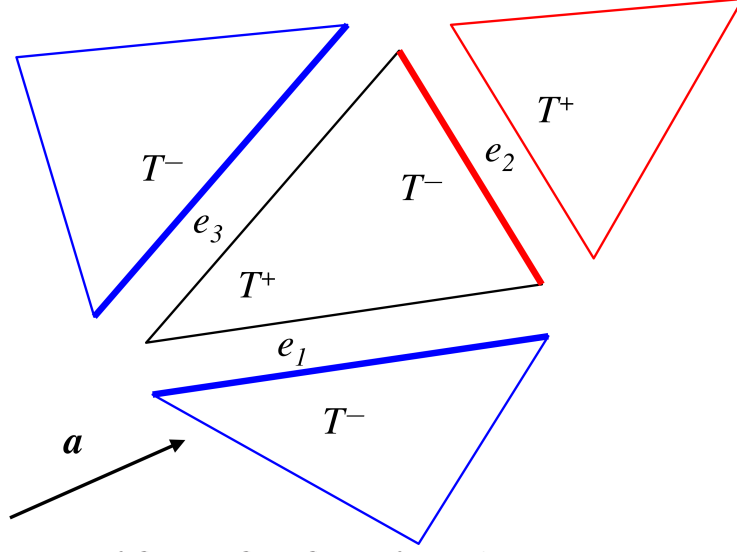


Figure 5: Local conservation of flux: inflow fluxes from the contiguous upwind elements (blue) are balanced by the outflow flux on the outflow boundary of the element (red).

the same place. A unique property of our DG formulation is the upwinding of the total flux. This results in locally conservative fluxes that are computed entirely in one place. To clarify this important distinction let us assume that T and \mathbf{a} are in the configuration shown in Fig. 5 and that the edges of T are numbered counterclockwise starting from the bottom edge. Let ϕ_h^T denote the value of ϕ_h on T and ϕ_h^C denote the value of this function on the contiguous elements. Then, the conserved flux is given by

$$\mathbf{a}\phi_h^- - \kappa\nabla\phi_h^- = \begin{cases} \mathbf{a}\phi_h^C - \kappa\nabla\phi_h^C & \text{on } e_1 \cup e_3 \\ \mathbf{a}\phi_h^T - \kappa\nabla\phi_h^T & \text{on } e_2 \end{cases} \quad (27)$$

From this it is clear that in our formulation the *outflow* fluxes on the outflow boundary of the element in question are balanced by the *inflow* fluxes from the *contiguous* upwind elements; see Fig. 5. This consistent upwinding of the flux is reminiscent of the consistent weighting of the residual in a stabilized method [10, 31, 34].

3.1.2 Euler-Lagrange equations

To understand (22), it is instructive to derive the Euler-Lagrange equations by means of an integration-by-parts. Use of (17) with $\boldsymbol{\tau} = \kappa\nabla\phi_h$ and (19) with $\boldsymbol{\tau} = \mathbf{a}\phi_h$ yields:

$$\begin{aligned} 0 &= \sum_{T \in \mathcal{T}_h} \int_T \mu_h (\nabla \cdot (\mathbf{a}\phi_h - \kappa\nabla\phi_h) - f) \\ &+ \sum_{e \in \Gamma_g} \int_e \left(\frac{\epsilon\kappa}{h_\perp} \mu_h + s\kappa\nabla\mu_h \cdot \mathbf{n} - \mu_h \mathbf{a}\chi_{\Gamma_g^-} \right) (\phi_h - g) \\ &+ \sum_{e \in \Gamma_h} \int_e \mu_h \left((-\mathbf{a}\phi_h \chi_{\Gamma_h^-} + \kappa\nabla\phi_h) \cdot \mathbf{n} - h \right) \\ &+ \sum_{e \in \mathcal{E}_h^o} \left(\int_e (-\mu_h^+ [\mathbf{a}\phi_h - \kappa\nabla\phi_h] + s\kappa\nabla\mu_h^- \cdot [\phi_h]) + \int_e \frac{\epsilon\kappa}{h_\perp} [\mu_h] \cdot [\phi_h] \right) \end{aligned} \quad (28)$$

Remarks

1. The first sum weakly enforces satisfaction of the advection-diffusion equation on each element domain T .
2. The terms multiplied by the parameter ϵ serve the purpose of eliminating a kernel in the discrete diffusive operator, in the limit $\mathbf{a} \rightarrow \mathbf{0}$.
3. In the second sum, Dirichlet boundary conditions are weakly enforced by weighting their residual $\phi_h - g$ by the total flux at the inflow and the diffusive flux at the outflow. In the advection-dominated limit, the outflow boundary condition is significantly relaxed, whereas when diffusion dominates, it converges toward strong satisfaction everywhere.
4. In the third sum, Neumann conditions are imposed according to the same rationale as for the Dirichlet conditions. The total flux $\mathbf{a}\phi_h - \kappa\nabla\phi_h$ is imposed at the inflow, while only the diffusive flux is specified at the outflow.
5. The first term in the last sum weakly enforces continuity of the total flux across internal element interfaces. It represents an upwinded total flux, since the jump of the fluxes upwind and downwind of an edge are weighted by the downwind test function μ_h^+ . The total flux is conserved and upwinded.
6. The terms involving $[[\phi_h]]$ weakly enforce the continuity of ϕ_h across element interfaces.

4 Local Weak Formulations

4.1 Local problem for the trial solution

The discontinuous field $\phi_h \in V_h^k$ is linked to a continuous field $\bar{\phi}_h \in \bar{V}_h^k$ by the following local (i.e., element-by-element) DG problem:

Find $\phi_h \in V_h^k(T)$ such that, $\forall v \in V_h^k(T)$:

$$\begin{aligned}
0 = & - \int_T \nabla v \cdot (\mathbf{a}\phi_h - \kappa\nabla\phi_h) - \int_T v f + \epsilon \int_{\Gamma_T} \frac{\tilde{\kappa}}{h_\perp} v (\phi_h - \bar{\phi}_h) \\
& + \int_{\Gamma_T^+} v \phi_h \mathbf{a} \cdot \mathbf{n} + \int_{\Gamma_T^-} v \bar{\phi}_h \mathbf{a} \cdot \mathbf{n} \\
& + \int_{\Gamma_T} s \kappa \nabla v \cdot \mathbf{n} (\phi_h - \bar{\phi}_h) - \int_{\Gamma_T} \kappa \nabla \phi_h \cdot \mathbf{n} v
\end{aligned} \tag{29}$$

where

$$\tilde{\kappa} = \kappa + \delta \chi_{\Gamma_T^+} h_\perp \mathbf{a} \cdot \mathbf{n} \tag{30}$$

and $V_h^k(T) = \mathcal{P}^k(T)$. The parameter δ eliminates a kernel which can occur in the limit $\kappa \rightarrow 0$ in isolated circumstances. Further discussion will be presented subsequently. The Euler-Lagrange equations are:

$$\begin{aligned}
0 = & \int_T v (\nabla \cdot (\mathbf{a}\phi_h - \kappa\nabla\phi_h) - f) + \epsilon \int_{\Gamma_T} \frac{\tilde{\kappa}}{h_\perp} v (\phi_h - \bar{\phi}_h) \\
& + \int_{\Gamma_T^-} v \mathbf{a} \cdot \mathbf{n} (\bar{\phi}_h - \phi_h) - \int_{\Gamma_T} s \kappa \nabla v \cdot \mathbf{n} (\bar{\phi}_h - \phi_h)
\end{aligned} \tag{31}$$

Equation (29) can be succinctly expressed as:

Find $\phi_h \in V_h^k(T)$ such that, $\forall v \in V_h^k(T)$:

$$B(v, \phi_h) = F(v; f, \bar{\phi}_h) \quad (32)$$

where

$$\begin{aligned} B(v, \phi_h) &= - \int_T \nabla v \cdot (\mathbf{a}\phi_h - \kappa \nabla \phi_h) - \int_{\Gamma_T} v \kappa \nabla \phi_h \cdot \mathbf{n} \\ &\quad + \int_{\Gamma_T} \left(\frac{\epsilon \tilde{\kappa}}{h_\perp} v + \left(s \kappa \nabla v + v \chi_{\Gamma_T^+} \mathbf{a} \right) \cdot \mathbf{n} \right) \phi_h \end{aligned} \quad (33)$$

$$F(v; f, \bar{\phi}_h) = \int_T v f + B_\Gamma(v, \bar{\phi}_h) \quad (34)$$

and

$$B_\Gamma(v, \bar{\phi}_h) = \int_{\Gamma_T} \left(\frac{\epsilon \tilde{\kappa}}{h_\perp} v + \left(s \kappa \nabla v - v \chi_{\Gamma_T^-} \mathbf{a} \right) \cdot \mathbf{n} \right) \bar{\phi}_h \quad (35)$$

$B(\cdot, \cdot)$ and $B_\Gamma(\cdot, \cdot)$ are bilinear forms and $F(\cdot; \cdot, \cdot)$ is linear with respect to its first argument and affine with respect to its second and third arguments. Let n_{en} denote the number of element nodes and let $\{\psi_j\}_1^{n_{en}}$ denote the nodal basis for the element in question. The basis functions associated with the element boundary nodes are denoted $\{\bar{\psi}_j\}_1^{\bar{n}_{en}}$. Obviously, these are a subset of $\{\psi_j\}_1^{n_{en}}$. We write

$$v = \sum_{j=1}^{n_{en}} v_j \psi_j \quad (36)$$

$$\phi_h = \sum_{j=1}^{n_{en}} \Phi_j \psi_j \quad (37)$$

$$\bar{\phi}_h = \sum_{j=1}^{\bar{n}_{en}} \bar{\Phi}_j \bar{\psi}_j \quad (38)$$

$$f = \sum_{j=1}^{n_{en}} f_j \psi_j \quad (39)$$

where v_j , Φ_j , and $\bar{\Phi}_j$, and f_j denote nodal values. The interpretation is that ϕ_h is the discontinuous solution and $\bar{\phi}_h$ is the continuous solution in which degrees-of-freedom are shared on element boundaries. Substitution into (32) yields a local algebraic problem:

$$\mathbf{S} \Phi = \bar{\mathbf{S}}_\Gamma \bar{\Phi} + \mathbf{M} \mathbf{f} \quad (40)$$

$$S_{ij} = B(\psi_i, \psi_j) \quad (41)$$

$$(\bar{\mathbf{S}}_\Gamma)_{ij} = B_\Gamma(\psi_i, \bar{\psi}_j) \quad (42)$$

$$M_{ij} = \int_T \psi_i \psi_j \quad (43)$$

where $\bar{\Phi} = [\bar{\Phi}_1, \bar{\Phi}_2, \dots, \bar{\Phi}_{\bar{n}_{en}}]^t$, $\Phi = [\Phi_1, \Phi_2, \dots, \Phi_{n_{en}}]^t$, and $\mathbf{f} = [f_1, f_2, \dots, f_{n_{en}}]^t$. Provided \mathbf{S} is invertible, it is possible to express Φ in terms of $\bar{\Phi}$ and \mathbf{f} :

$$\Phi = \mathbf{T}_{\phi_h \bar{\phi}_h}^h \bar{\Phi} + \mathbf{T}_{\phi_h f}^h \mathbf{f} \quad (44)$$

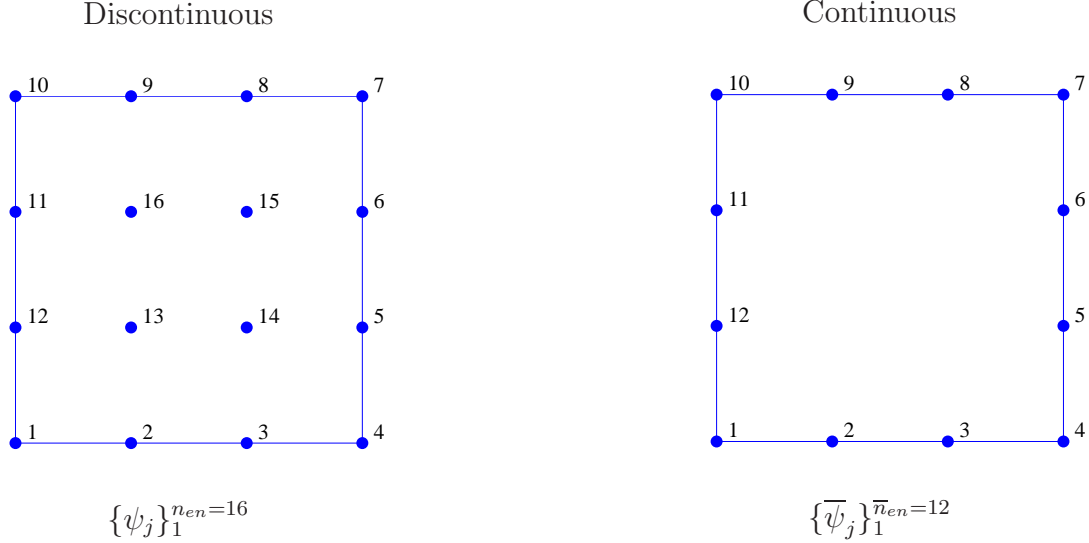


Figure 6: Schematic illustration of the basis functions in the local problem. On the left is a 16-node bicubic quadrilateral element. Its boundary nodes are identified on the right. The corresponding basis functions satisfy $\bar{\psi}_j = \psi_j$, $j = 1, 2, \dots, 12$. The internal degrees-of-freedom, corresponding to ψ_{13} , ψ_{14} , ψ_{15} , ψ_{16} , are eliminated by the solution of the local problem. Only the unique, shared, boundary degrees-of-freedom are retained in the global problem.

where $\mathbf{T}_{\phi_h \bar{\phi}_h}^h = \mathbf{S}^{-1} \bar{\mathbf{S}}_\Gamma$ and $\mathbf{T}_{\phi_h f}^h = \mathbf{S}^{-1} \mathbf{M}$. This mapping enables us to eliminate local degrees-of-freedom in favor of global degrees-of-freedom. See Figure 6.

4.1.1 Multiscale interpretation

Let $\phi_h = \bar{\phi}_h + \phi'_h$. We think of $\bar{\phi}_h \in \bar{V}_h^k$ as the coarse-scale component of the solution, and $\phi'_h \in V_h^k$ as the fine-scale component. By virtue of the fact that $\bar{\phi}_h$ is continuous, ϕ'_h may be thought of as the discontinuous part of the solution. Thus, the local problem can be stated as:

Find $\phi'_h \in V_h^k(T)$ such that, $\forall v \in V_h^k(T)$:

$$B(v, \phi'_h) = R(v; f, \bar{\phi}_h) \quad (45)$$

where

$$\begin{aligned} R(v; f, \bar{\phi}_h) &= F(v; f, \bar{\phi}_h) - B(v, \bar{\phi}_h) \\ &= \int_T (\nabla v \cdot (\mathbf{a} \bar{\phi}_h - \kappa \nabla \bar{\phi}_h) + v f) - \int_{\Gamma_T} v (\mathbf{a} \bar{\phi}_h - \kappa \nabla \bar{\phi}_h) \cdot \mathbf{n} \\ &= - \int_T v (\mathbf{a} \cdot \nabla \bar{\phi}_h - \kappa \Delta \bar{\phi}_h - f) \end{aligned} \quad (46)$$

is the residual of the coarse-scale solution. Comparing (46) with (33) and (34), it is immediately realized that the local problem for the discontinuous correction ϕ'_h corresponds to a local DG method with weakly-enforced homogeneous Dirichlet boundary conditions, driven by the residual. The relationship with the multiscale analysis presented in Hughes [31] and Hughes *et al.* [33] is then evident.

The local algebraic problem becomes

$$\mathbf{S} \boldsymbol{\Phi}' = \overline{\mathbf{S}}_\Gamma \overline{\boldsymbol{\Phi}} - \overline{\mathbf{S}} \overline{\boldsymbol{\Phi}} + \mathbf{M} \mathbf{f} \quad (47)$$

where

$$\overline{\mathbf{S}}_{ij} = B(\psi_i, \overline{\psi}_j) \quad (48)$$

leading to

$$\boldsymbol{\Phi}' = \mathbf{T}_{\phi'_h \overline{\phi}_h}^h \overline{\boldsymbol{\Phi}} + \mathbf{T}_{\phi_h f}^h \mathbf{f} \quad (49)$$

in which

$$\mathbf{T}_{\phi'_h \overline{\phi}_h}^h = \mathbf{T}_{\phi_h \overline{\phi}_h}^h - \mathbf{S}^{-1} \overline{\mathbf{S}} \quad (50)$$

Remark

If there are no element internal degrees-of-freedom, that is if $\overline{\psi}_j = \psi_j, \forall j$, which is typically the case for low-order elements, then $\overline{\mathbf{S}} = \mathbf{S}$.

4.2 Local problem for the weighting function

The discontinuous weighting function $\mu_h \in V_h^k$ is also linked to the continuous weighting function $\overline{\mu}_h \in \overline{V}_h^k$ as follows:

Find $\mu_h \in V_h^k(T)$ such that, $\forall v \in V_h^k(T)$:

$$B(v, \mu_h) = F(v; 0, \overline{\mu}_h) \quad (51)$$

The multiscale version is given by

Find $\mu'_h \in V_h^k(T)$ such that, $\forall v \in V_h^k(T)$:

$$B(v, \mu'_h) = R(v; 0, \overline{\mu}_h) \quad (52)$$

Remarks

1. The introduction of the local problems is seen to eliminate the fine-scale degrees-of-freedom in favor of the coarse-scale degrees-of-freedom. The combination of the local and global weak formulations defines the new MDG method.
2. The present approach has some similarities to the variational multiscale method [31, 33] and the residual-free bubble (RFB) method [6, 9]. There are many variants of these procedures. Perhaps the one which is the closest to the present work is the discontinuous residual-free bubble (DRFB) method of Sangalli [47]. As is typical in RFB methods, Sangalli begins with the standard weak form. Both the finite element and bubble spaces are normally assumed to be conforming but, inspired by [9], in which a discontinuous approximation of the exact bubble is shown to work well in the advection-dominated limit, Sangalli proposes a discontinuous Galerkin formulation of the local problem. There are three ostensible differences between DRFB and the present approach: (1) The global formulation in DRFB derives from the *continuous* Galerkin method, whereas ours derives from the *discontinuous* Galerkin method; (2) DRFB focuses only on the advection-dominated case

and does not deal with some of the issues concerning the local problem that we considered, namely, the diffusion-dominated regime, and transition regime where both advective and diffusive mechanisms are important; and (3) the treatment of the weighting function in equation (52) has a substantial effect in the present approach but has no effect whatsoever in the RFB method. Despite these differences, the similarities are intriguing and warrant further investigation.

5 Numerical Results

5.1 One-dimensional advection-diffusion

We assume the advective velocity, a , is positive and constant, and the force, f is constant. The exact solution of the strong form (7) is easily derived:

$$\phi(x) = \phi_0 + (\phi_L - \phi_0) \frac{1 - e^{Pe_L \frac{x}{L}}}{1 - e^{Pe_L}} + \frac{2\mathcal{F}}{Pe_L} \left(\frac{x}{L} - \frac{1 - e^{Pe_L \frac{x}{L}}}{1 - e^{Pe_L}} \right) \quad (53)$$

where ϕ_0 and ϕ_L are Dirichlet boundary conditions imposed at $x = 0$ and $x = L$, $Pe_L = aL/\kappa$ is the Péclet number, and $\mathcal{F} = fL^2/(2\kappa)$ is the source. In the limit $Pe_L \rightarrow 0$, (53) yields:

$$\phi(x) = \phi_0 + (\phi_L - \phi_0 + \mathcal{F}) \frac{x}{L} - \mathcal{F} \left(\frac{x}{L} \right)^2 \quad (54)$$

5.1.1 Weak formulation

It is now worthwhile to recast (22) for the case at hand because many simplifications arise.

Find $\phi_h \in V_h^k([x_e, x_{e+1}])$, $e \in \{1, 2, \dots, n_{el}\}$, such that, $\forall \mu_h \in V_h^k([x_e, x_{e+1}])$:

$$\begin{aligned} 0 = & - \sum_{e=1}^{n_{el}} \int_{x_e}^{x_{e+1}} (\partial_x \mu_h (a\phi_h - \kappa \partial_x \phi_h) + \mu_h f) \\ & + \sum_{e=2}^{n_{el}} \left\{ (-\mu_h^+ + \mu_h^-)(a\phi_h^- - \kappa \partial_x \phi_h^-) + \left(s \kappa \partial_x \mu_h^- + \epsilon \frac{\kappa}{h_\perp} (-\mu_h^+ + \mu_h^-) \right) (-\phi_h^+ + \phi_h^-) \right\}_{x=x_e} \\ & + \left\{ +\mu_h a\phi_h + \epsilon \frac{\kappa}{h_\perp} \mu_h (\phi_h - \phi_L) + s \kappa \partial_x \mu_h (\phi_h - \phi_L) - \kappa \partial_x \phi_h \mu_h \right\}_{x=L} \\ & + \left\{ -\mu_h a\phi_0 + \epsilon \frac{\kappa}{h_\perp} \mu_h (\phi_h - \phi_0) - s \kappa \partial_x \mu_h (\phi_h - \phi_0) + \kappa \partial_x \phi_h \mu_h \right\}_{x=0} \end{aligned} \quad (55)$$

where the notation $\{\eta\}_{x=\tilde{x}}$ stands for η evaluated at \tilde{x} , $e \in \{1, 2, \dots, n_{np}\}$ are the nodes of the mesh, and $\{x_e \mid e = 2, \dots, n_{np} - 1 = n_{el}\}$ is the set of interior nodes.

5.1.2 Local problem for the trial solution

The local problem reads:

$$B(v, \phi_h) = F(v; f, \bar{\phi}_h) \quad (56)$$

with

$$\begin{aligned}
B(v, \phi_h) &= - \int_{x_e}^{x_{e+1}} \partial_x v (a\phi_h - \kappa \partial_x \phi_h) \\
&\quad + \left\{ v a\phi_h + \epsilon \frac{\tilde{\kappa}}{h_\perp} v \phi_h + s \kappa \partial_x v \phi_h - \kappa \partial_x \phi_h v \right\}_{x=x_{e+1}} \\
&\quad + \left\{ \epsilon \frac{\tilde{\kappa}}{h_\perp} v \phi_h - s \kappa \partial_x v \phi_h + \kappa \partial_x \phi_h v \right\}_{x=x_e}
\end{aligned} \tag{57}$$

$$F(v; f, \bar{\phi}_h) = \int_T v f + B_\Gamma(v, \bar{\phi}_h) \tag{58}$$

$$\begin{aligned}
B_\Gamma(v, \bar{\phi}_h) &= + \left\{ \epsilon \frac{\tilde{\kappa}}{h_\perp} v \bar{\phi}_h + s \kappa \partial_x v \bar{\phi}_h \right\}_{x=x_{e+1}} \\
&\quad + \left\{ -v a\bar{\phi}_h + \epsilon \frac{\tilde{\kappa}}{h_\perp} v \bar{\phi}_h - s \kappa \partial_x v \bar{\phi}_h \right\}_{x=x_e}
\end{aligned} \tag{59}$$

Piecewise linear interpolation is assumed. Let

$$\Phi = \begin{bmatrix} \phi_h^l \\ \phi_h^r \end{bmatrix}, \quad \bar{\Phi} = \begin{bmatrix} \bar{\phi}_h^l \\ \bar{\phi}_h^r \end{bmatrix}, \quad \mathbf{f} = \begin{bmatrix} f^l \\ f^r \end{bmatrix} \tag{60}$$

where the superscripts l and r stand for the left and right nodal values. Straightforward calculations yield

$$\mathbf{T}_{\phi_h \bar{\phi}_h}^h = \frac{1}{\Delta} \begin{bmatrix} t_{11} & t_{12} \\ t_{21} & t_{22} \end{bmatrix} \tag{61}$$

with

$$\Delta = (Pe_h)^2(1 + \delta\epsilon) + (s + \epsilon)(1 + \delta\epsilon)Pe_h + \epsilon/2(2s + \epsilon) \tag{62}$$

$$t_{11} = (Pe_h)^2(1 + 2\delta\epsilon) + (s(2 + \delta\epsilon) + \epsilon/2(3 + 2\delta\epsilon))Pe_h + \epsilon/2(2s + \epsilon) \tag{63}$$

$$t_{12} = -Pe_h(Pe_h\delta\epsilon + s + \epsilon/2) \tag{64}$$

$$t_{21} = Pe_h(Pe_h\delta\epsilon + s + \epsilon/2) \tag{65}$$

$$t_{22} = \epsilon((Pe_h)^2\delta + Pe_h(1/2 + \delta(s + \epsilon)) + s + \epsilon/2) \tag{66}$$

$$Pe_h = \frac{ah}{2\kappa} \tag{67}$$

and

$$\mathbf{T}_{\phi_h f}^h = \frac{h^2}{12\kappa\Delta} \begin{bmatrix} Pe_h(1 + \delta\epsilon) + 3s + 2\epsilon & -Pe_h(1 - 2\delta\epsilon) + 3s + \epsilon \\ 3Pe_h + 3s + \epsilon & 3Pe_h + 3s + 2\epsilon \end{bmatrix} \tag{68}$$

Special care has to be taken because, for $s = -1$, the determinant, Δ , can vanish for certain combinations of Pe_h and ϵ . An analysis of the sign of the determinant is presented in Table 1. The locus of $\Delta = 0$ in the Pe_h, ϵ -plane is shown in Figure 7, together with an elevation plot of the function $\Delta(Pe_h, \epsilon)$. In the multiscale version, $\mathbf{T}_{\phi_h' \bar{\phi}_h}^h = \mathbf{T}_{\phi_h \bar{\phi}_h}^h - \mathbf{I}_{2 \times 2}$.

	$s = +1$	$s = 0$	$s = -1$
Δ	$Pe_h(Pe_h + 1) + \epsilon(Pe_h + 1) + \epsilon^2/2$	$(Pe_h)^2 + (Pe_h + \epsilon)^2$	$Pe_h(Pe_h - 1) + \epsilon(Pe_h - 1) + \epsilon^2/2$
$\Delta > 0?$	always for $\epsilon > 0$	always for $\epsilon > 0$	for $\epsilon > 1 - Pe_h + \sqrt{1 - Pe_h^2}$ and $\epsilon < 1 - Pe_h - \sqrt{1 - Pe_h^2}$

Table 1: Analysis of the sign of the determinant Δ for $\delta = 0$.

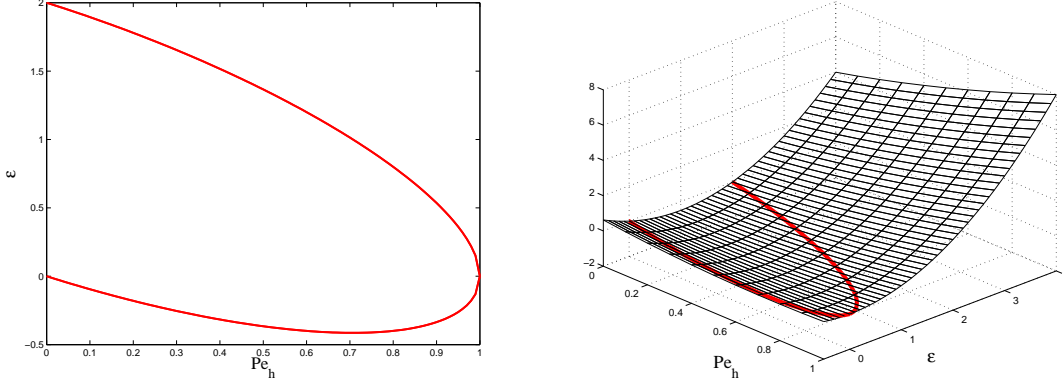


Figure 7: Locus of $\Delta = 0$ for $s = -1$ and $\delta = 0$ on the Pe_h, ϵ -plane (left) and on an elevation plot of the function Δ . It is seen that $\epsilon > 2$ prevents the determinant from vanishing for all Péclet numbers.

5.1.3 Limit behavior

Taking limits, $Pe_h \rightarrow 0$ and ∞ , we have:

$$\lim_{Pe_h \rightarrow 0} \mathbf{T}_{\phi_h \bar{\phi}_h}^h = \begin{bmatrix} 1 & 0 \\ 0 & 1 \end{bmatrix} \quad (69)$$

$$\lim_{Pe_h \rightarrow \infty} \mathbf{T}_{\phi_h \bar{\phi}_h}^h = \frac{1}{1 + \delta\epsilon} \begin{bmatrix} 1 + 2\delta\epsilon & -2\delta\epsilon \\ 1 & \delta\epsilon \end{bmatrix} \quad (70)$$

$$\lim_{Pe_h \rightarrow 0} \mathbf{T}_{\phi_h f}^h = \frac{h}{6\kappa\epsilon(2s + \epsilon)} \begin{bmatrix} 3s + 2\epsilon & 3s + \epsilon \\ 3s + \epsilon & 3s + 2\epsilon \end{bmatrix} \quad (71)$$

$$\lim_{Pe_h \rightarrow \infty} \mathbf{T}_{\phi_h f}^h = \mathbf{0}_{2 \times 2} \quad (72)$$

From (69) it is seen that, if $f = 0$, $\phi_h \rightarrow \bar{\phi}_h$ in the diffusive limit, while from (70) it is seen that, in the advective limit, full upwinding is performed up to the perturbation of the parameter δ , that is $\phi_h|_{[x_e, x_{e+1}]} \rightarrow \bar{\phi}_h(x_e)\chi|_{[x_e, x_{e+1}]}$, for a positive. Notice also that, due to the fact that in the diffusive limit $\mathbf{T}_{\phi_h f}^h$ does not vanish, the continuous solution, $\bar{\phi}_h$, will not in general be equal to the discontinuous solution, ϕ_h , when f is present. The behavior of the method is schematically illustrated in Figure 8.

Note that, in the advective limit, $Pe_h \rightarrow \infty$, without the δ -term, the transformation $T_{\phi_h \bar{\phi}_h}$ becomes singular and the global coefficient matrix entries corresponding to the degree-of-freedom

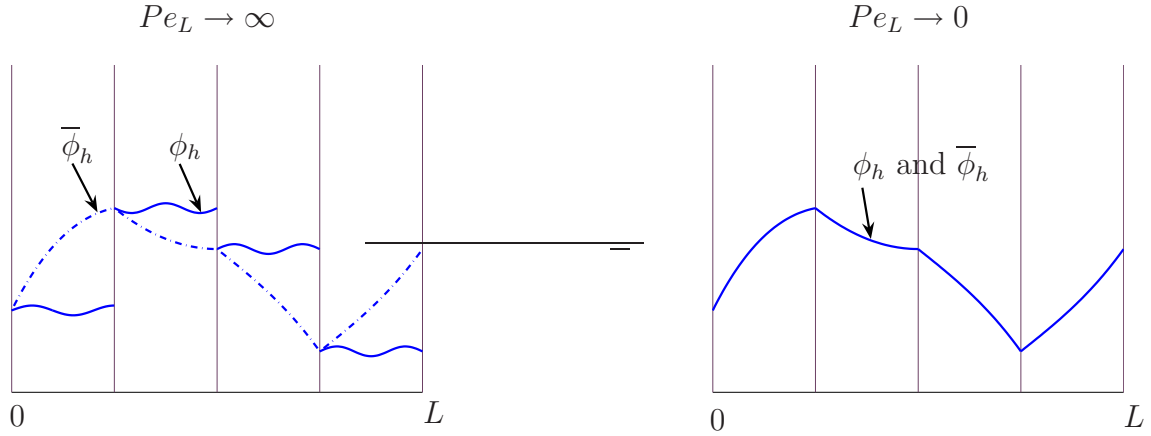


Figure 8: Schematic of the behavior of the new method. In the advective limit, the solution exhibits upwind influence, whereas in the diffusive limit the solution behaves like the continuous solution although it is not identical to it in the case $f \neq 0$.

$\bar{\phi}_h^r$ will receive no contribution from the element under consideration. If the node associated with this degree-of-freedom is an outflow node with respect to all elements connected to it, the global coefficient matrix will have a zero row and column corresponding to this degree-of-freedom. Situations where this can occur are schematically illustrated in Figure 9. The role of the δ -term is to provide stabilization in these circumstances. In all numerical tests, this strategy has proved effective.

5.1.4 Local problem for the weighting function

Given that the problem of linking μ_h to $\bar{\mu}_h$ is the same as for linking ϕ_h to $\bar{\phi}_h$, except $f = 0$, the result is

$$\begin{bmatrix} \mu_h^l \\ \mu_h^r \end{bmatrix} = \mathbf{T}_{\mu_h \bar{\mu}_h}^h \begin{bmatrix} \bar{\mu}_h^l \\ \bar{\mu}_h^r \end{bmatrix} \quad (73)$$

or

$$\begin{bmatrix} \mu_h^l \\ \mu_h^r \end{bmatrix} = \mathbf{T}_{\mu_h' \bar{\mu}_h}^h \begin{bmatrix} \bar{\mu}_h^l \\ \bar{\mu}_h^r \end{bmatrix} \quad (74)$$

with $\mathbf{T}_{\mu_h \bar{\mu}_h}^h = \mathbf{T}_{\phi_h \bar{\phi}_h}^h$ and $\mathbf{T}_{\mu_h' \bar{\mu}_h}^h = \mathbf{T}_{\phi_h' \bar{\phi}_h}^h$.

5.1.5 Numerical results

We compare the continuous and discontinuous representations of the solution for the MDG formulation (i.e., $\bar{\phi}_h$ and ϕ_h , resp.) with the solution of the global DG method. We examine the effect of the parameter s on monotonicity of the solution, and convergence rates. The value $\epsilon = 2.001$ was used in the calculations. This value is essential for the good behavior of the symmetric case (i.e., $s = -1$). The parameter $\delta = 0.01$ was used throughout. Smaller values were not as effective.

In Figures 10 and 11, results are presented for a fixed, uniform mesh of four elements, and various Péclet numbers. One notices oscillations for the discontinuous representation of the solution, ϕ_h , for skew and neutral cases at intermediate Péclet numbers. The discontinuous

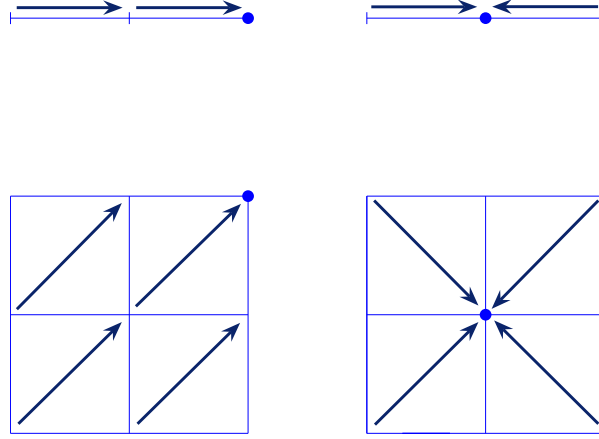


Figure 9: In the advective limit, outflow and sink nodes are stabilized by the δ -term. Strictly speaking, the sink-node cases are precluded by our assumption that \mathbf{a} is solenoidal. Nevertheless, in numerical calculations \mathbf{a} will also be a discrete approximation and therefore it will typically not be exactly solenoidal. See Hughes and Wells [38] for a discussion of this issue.

solutions for the symmetric case are oscillation-free and monotone for all Péclet numbers. The global DG solution is about the same quality as the discontinuous solution of the MDG method.

In Figure 12 and 13, results are presented for a fixed Péclet number, Pe_L , and varying mesh size. The conclusions to be drawn are similar to those of Figures 10 and 11. In all cases, the continuous representation of the solution for the MDG method, $\bar{\phi}_h$, tends to be somewhat better behaved than the discontinuous representation.

L^2 -convergence rates for the case $f = 0$ are presented in Figures 14–16. The first thing one notices is that in Figures 14–15, for the skew and neutral versions, the L^2 -convergence rates for the global DG method are first-order. This is to be expected because these methods are not adjoint consistent (see Arnold *et al.* [3]). The symmetric version is adjoint consistent, and so it converges at optimal L^2 -rate, as seen in Figure 16. For the present formulation, for *all* values of s , optimal L^2 -convergence is attained. This is seen to be a consequence of the fact that, in the diffusive limit, the discontinuous solution converges to the continuous solution, which is well-known to attain optimal L^2 -rate of convergence. The local problem has beneficial effect and compensates for the lack of adjoint consistency of the skew and neutral versions.

L^2 , H^1 , and L^1 , convergence rates are presented in Figures 17–19 for the case $f = 1$ and the symmetric version. By H^1 -convergence we mean convergence in the “broken” H^1 -seminorm, namely, $\sum_{T \in \mathcal{T}_h} \int_T |\nabla \cdot |^2$.

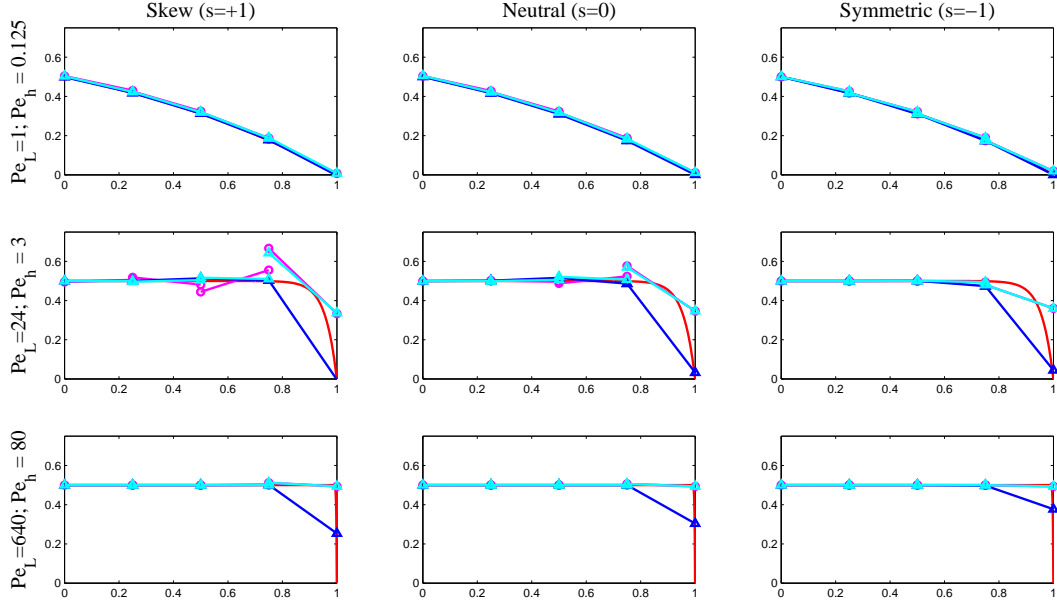


Figure 10: Solution plots in terms of varying Péclet number, on a uniform mesh of 4 elements, with $f = 0$. Red, exact solution; blue, MDG $\bar{\phi}_h$; light blue, MDG ϕ_h ; magenta, global DG solution without local condensation.

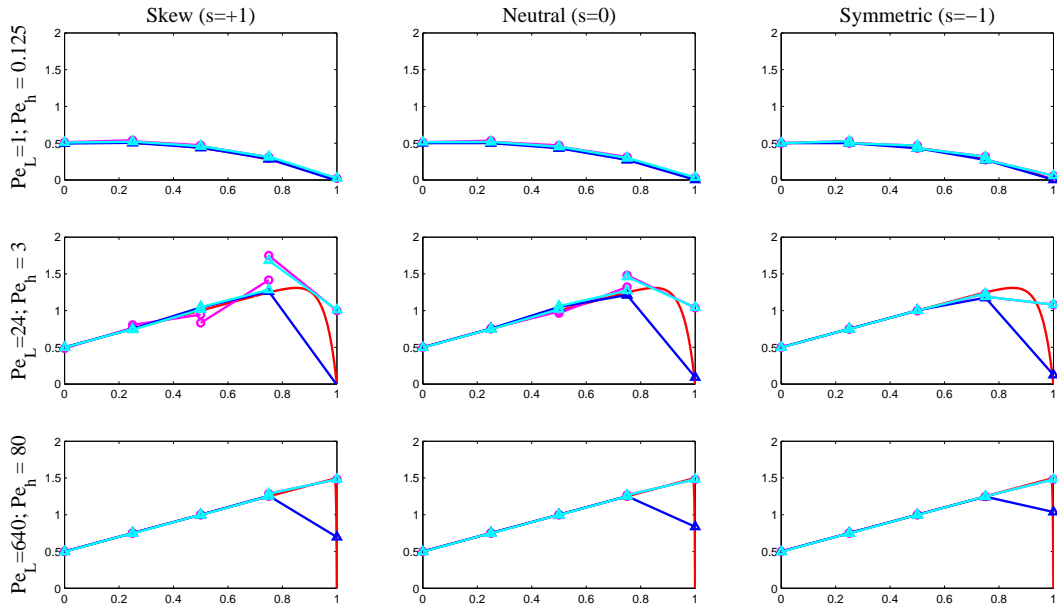


Figure 11: Solution plots in terms of varying Péclet number, on a uniform mesh of 4 elements, with $f = 1$. Red, exact solution; blue, MDG $\bar{\phi}_h$; light blue, MDG ϕ_h ; magenta, global DG solution without local condensation.

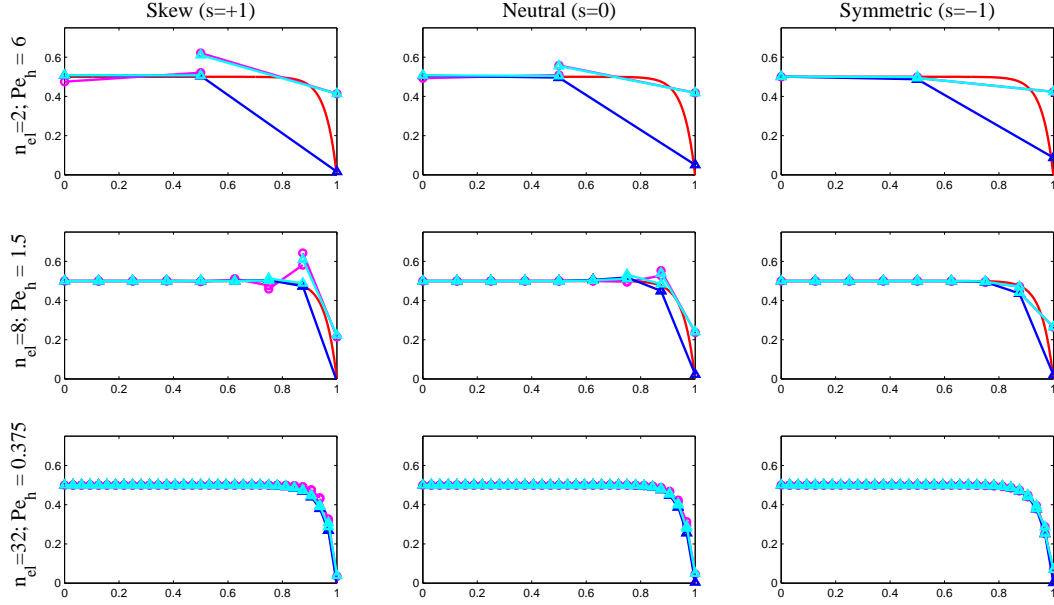


Figure 12: Solution plots in terms of varying mesh size, on uniform meshes of 2, 8, and 32 elements, $Pe_L = 24$, with $f = 0$. Red, exact solution; blue, MDG $\overline{\phi}_h$; light blue, MDG ϕ_h ; magenta, global DG solution without local condensation.

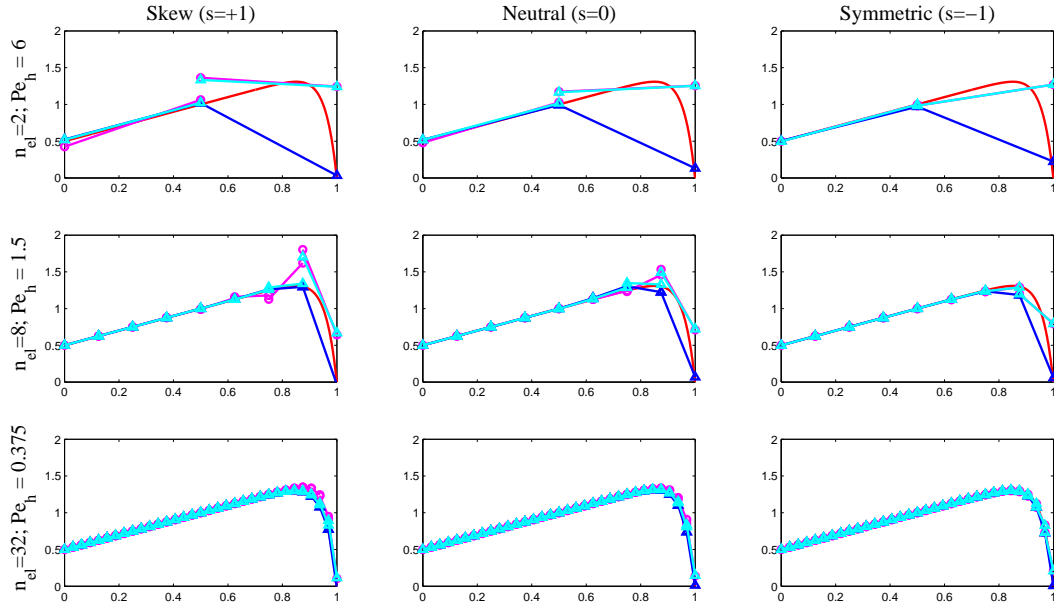


Figure 13: Solution plots in terms of varying mesh size, on uniform meshes of 2, 8, and 32 elements, $Pe_L = 24$, with $f = 1$. Red, exact solution; blue, MDG $\overline{\phi}_h$; light blue, MDG ϕ_h ; magenta, global DG solution without local condensation.

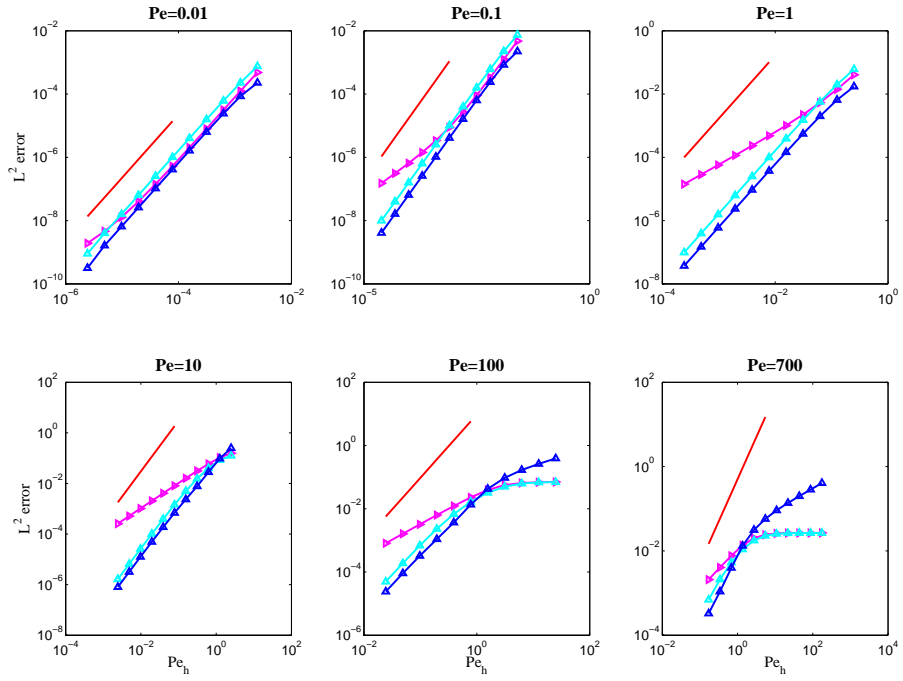


Figure 14: Convergence rates, skew ($s = +1$) version, with $f = 0$. Blue, MDG $\bar{\phi}_h$; light blue, MDG ϕ_h ; magenta, global DG solution without local condensation; red, $(Pe_h)^2$ slope.

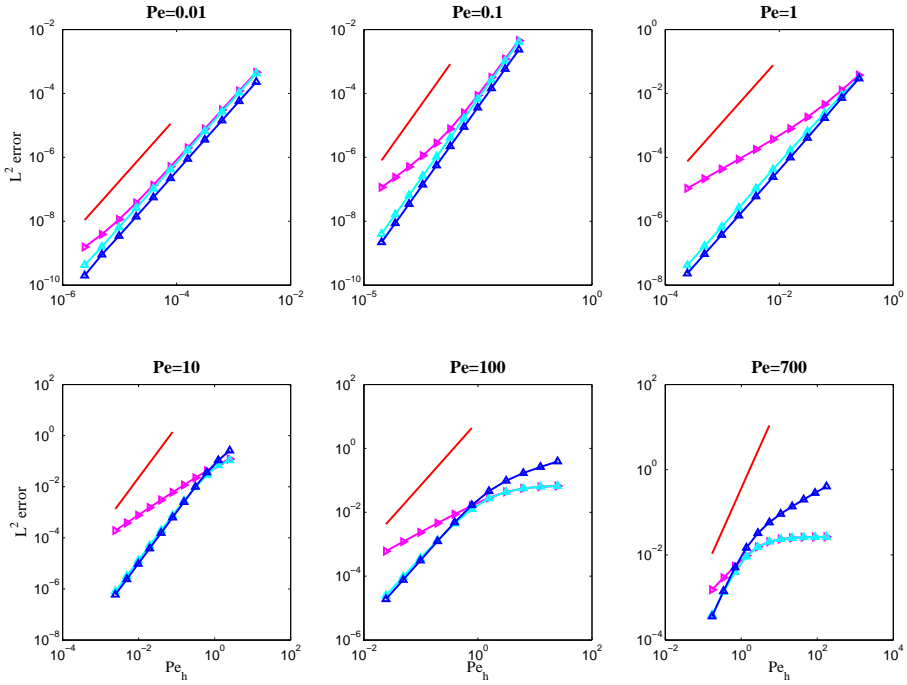


Figure 15: Convergence rates, neutral ($s = 0$) version, with $f = 0$. Blue, MDG $\bar{\phi}_h$; light blue, MDG ϕ_h ; magenta, global DG solution without local condensation; red, $(Pe_h)^2$ slope.

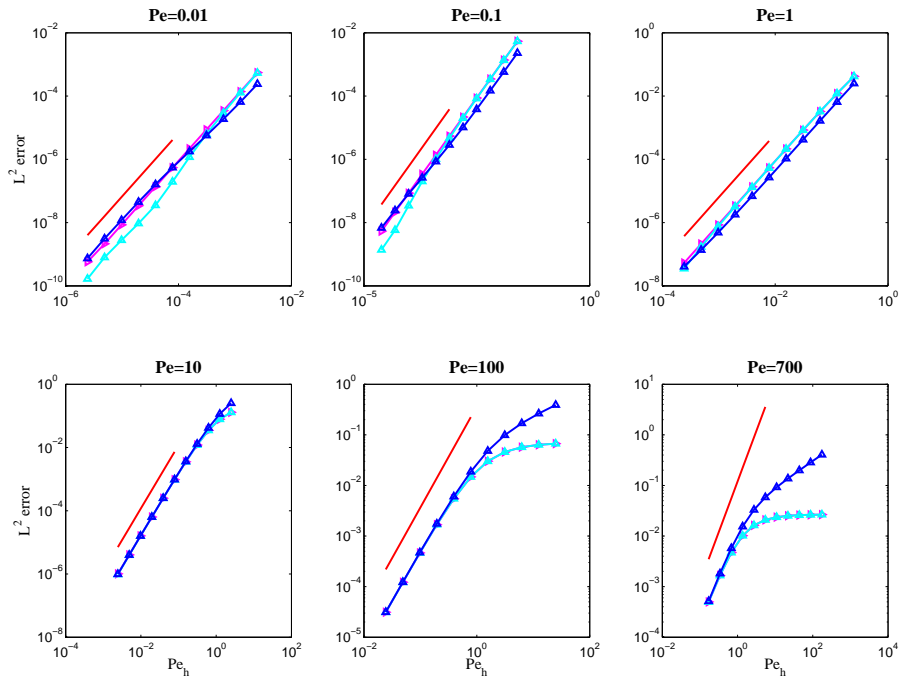


Figure 16: Convergence rates, symmetric ($s = -1$) version, with $f = 0$. Blue, MDG $\overline{\phi}_h$; light blue, MDG ϕ_h ; magenta, global DG solution without local condensation; red, $(Pe_h)^2$ slope.

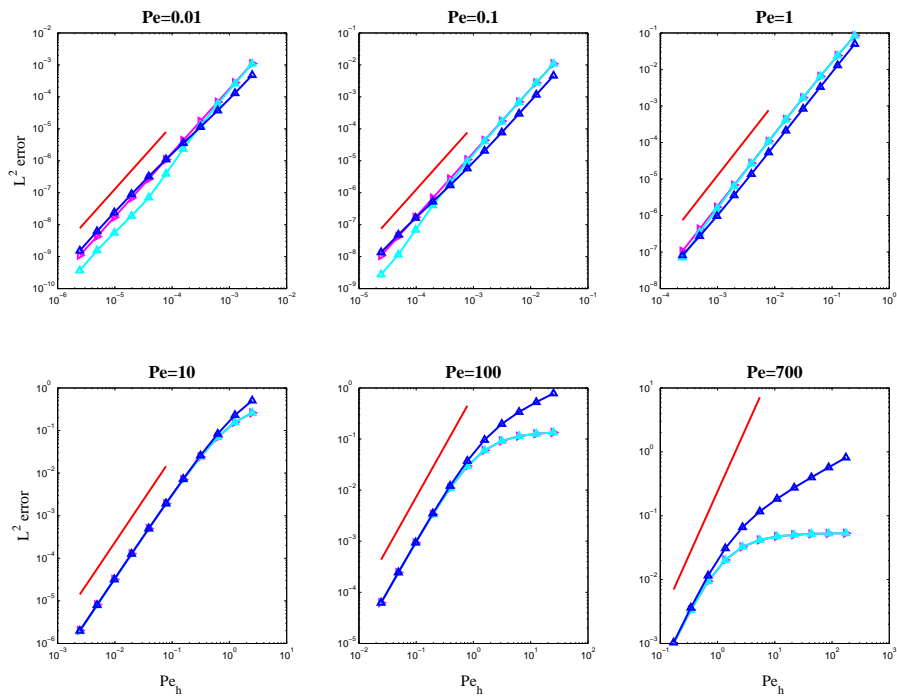


Figure 17: Convergence rates in the L^2 -norm of the error, symmetric ($s = -1$) version, with $f = 1$. Blue, MDG $\bar{\phi}_h$; light blue, MDG ϕ_h ; magenta, global DG solution without local condensation; red, $(Pe_h)^2$ slope.

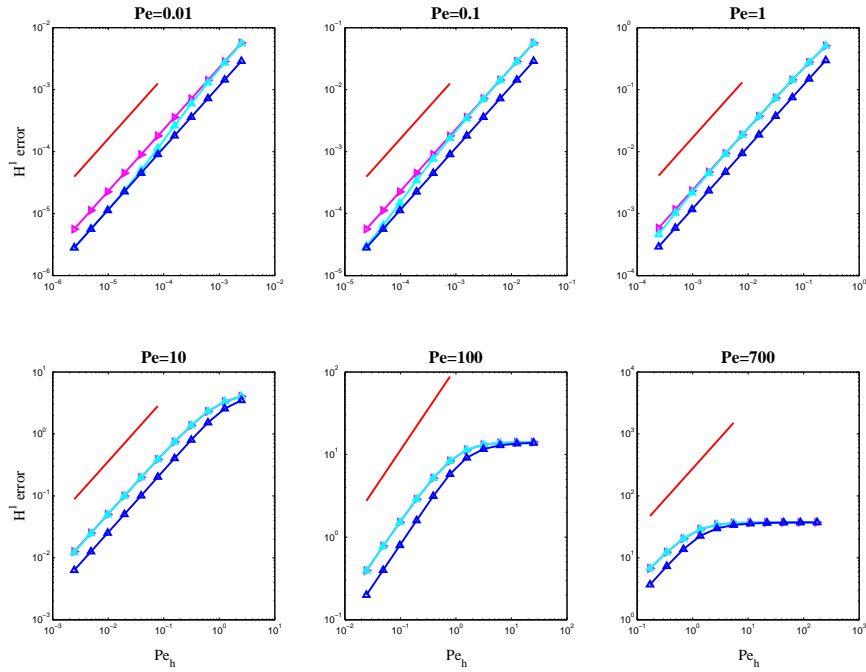


Figure 18: Convergence rates in the H^1 broken seminorm of the error, symmetric ($s = -1$) version, with $f = 1$. Blue, MDG $\bar{\phi}_h$; light blue, MDG ϕ_h ; magenta, global DG solution without local condensation; red, $(Pe_h)^1$ slope.

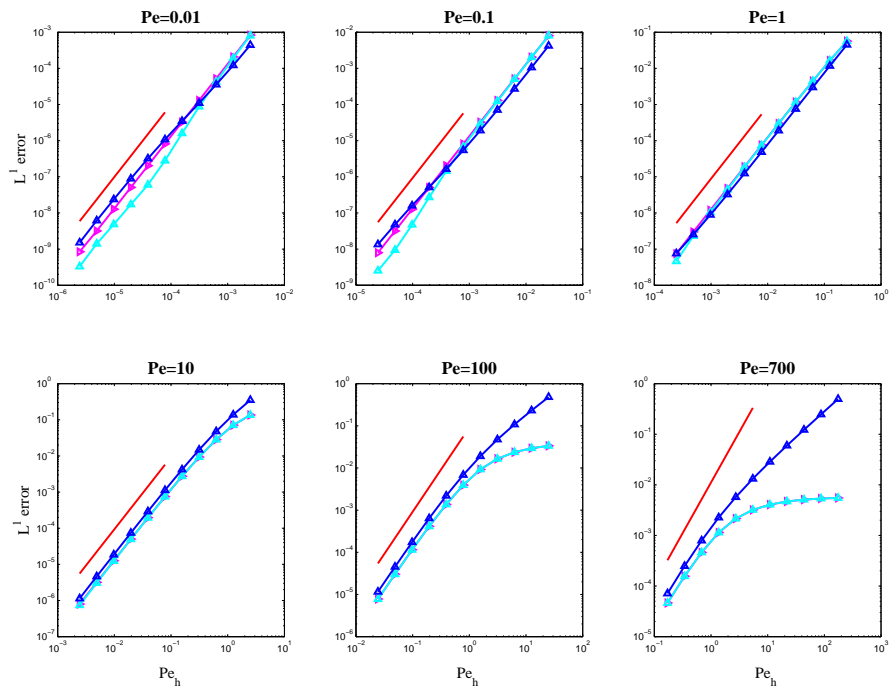


Figure 19: Convergence rates in the L^1 -norm of the error, symmetric ($s = -1$) version, with $f = 1$. Blue, MDG $\bar{\phi}_h$; light blue, MDG ϕ_h ; magenta, global DG solution without local condensation; red, $(Pe_h)^2$ slope.

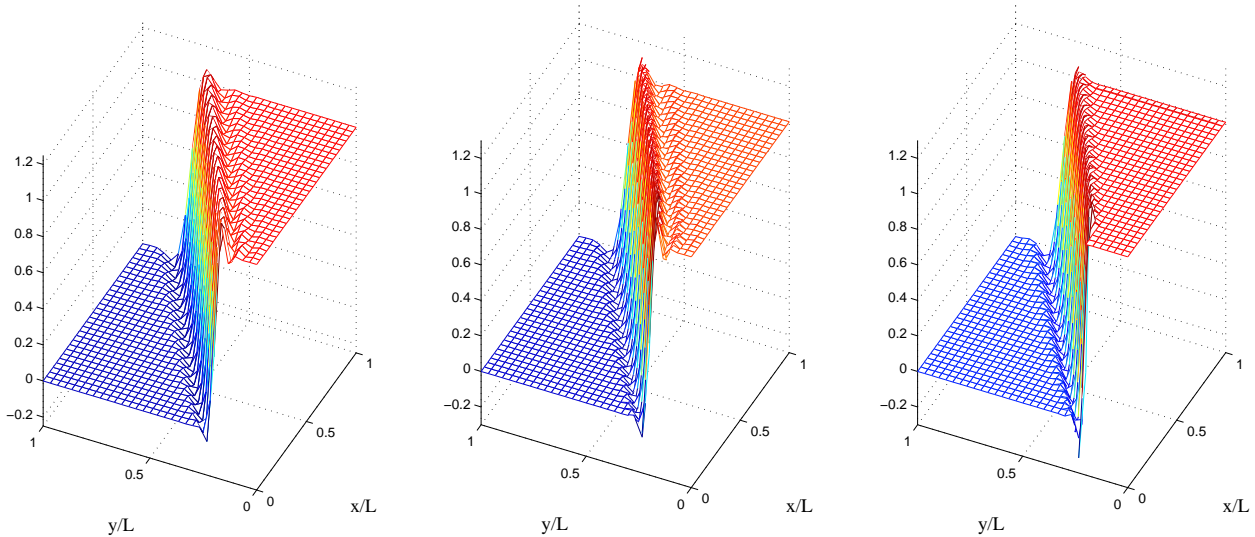


Figure 20: Advection skew to the mesh, $\theta = 30^\circ$. Left, continuous representation of the MDG solution, $\bar{\phi}_h$; center, discontinuous representation, ϕ_h ; right, solution of the global DG method without local condensation.

5.2 Two-dimensional advection equation

Two-dimensional simulations were performed to test the robustness and accuracy of the MDG method in the advection-dominated limit, $\kappa \rightarrow 0$. Comparisons are again made with the global DG method. Bilinear quadrilateral elements are employed resulting in the number of equations for the global DG method being approximately four times that for the MDG method. The symmetric version of the DG method was used ($s = -1$), and the values of ε and δ were again taken to be 2.001 and 0.01, respectively.

5.2.1 Advection skew to the mesh

The first problem is a robustness test. The domain of the problem is $\Omega = [0, L] \times [0, L]$ with $L = 1$. Dirichlet boundary conditions are set as follows:

$$g = \begin{cases} 1 & \text{if } y = 0 \\ 1 & \text{if } x = 0 \text{ and } y \leq L/5 \\ 0 & \text{otherwise} \end{cases} \quad (75)$$

The boundary conditions are enforced weakly for both the global and multiscale DG methods. The advective velocity \mathbf{a} is constant and forms an angle θ with the x -axis. Three configurations are considered: $\theta = 30^\circ$, $\theta = 45^\circ$ and $\theta = 60^\circ$ degrees.

Numerical results for a 30×30 mesh are presented in Figures 20–25. Note that the continuous representation of the solution, $\bar{\phi}_h$, is slightly better behaved than the discontinuous representation, ϕ_h , in that oscillations about the internal layer are somewhat less for the former. Comparison of the MDG solution with the global DG solution reveals that the multiscale method is similar in accuracy to the global method. The main attribute of both methods is that there are no spurious oscillations in the vicinity of the outflow boundary conditions. This is an advantage attributable to weakly enforced outflow boundary conditions, and one not shared by

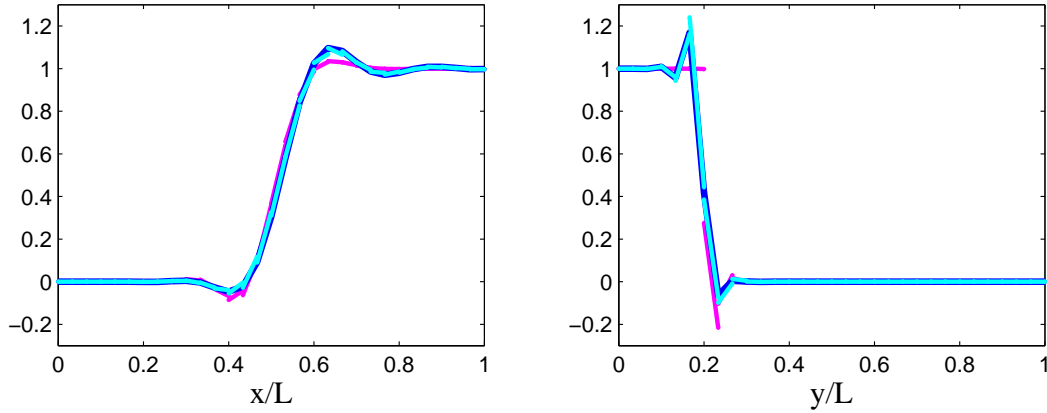


Figure 21: Advection skew to the mesh, $\theta = 30^\circ$. Left, solution at $y/L = .5$; right, solution at $x/L = 0$. Blue, MDG $\bar{\phi}_h$; light blue, MDG ϕ_h ; magenta, global DG solution without local condensation.

strong enforcement (see Brooks and Hughes [10]). However, weak enforcement of inflow Dirichlet boundary conditions offers no similar advantage over strong enforcement. Both the global and multiscale DG methods give rise to oscillations at the inflow discontinuity that attenuates somewhat in the interior of the domain. These oscillations are caused by the L^2 -projection structure of DG methods for data perpendicular to characteristics, such as the inflow boundary condition in the present problem. It is conceivable that, by appropriately restructuring the local problem, more monotone behavior might have been obtained but this was not pursued in the present study.

5.2.2 Rotating flow

This problem is an accuracy test. Classical upwind procedures exhibit excessive crosswind diffusion on this problem (see Brooks and Hughes [10]). The domain is again $\Omega = [0, L] \times [0, L]$ with $L = 1$. The two velocity components are:

$$a_x = y - 1/2 \quad (76)$$

$$a_y = 1/2 - x \quad (77)$$

The solution is prescribed along the slit $x = L/2$, $y \in [0, L/2]$, as follows:

$$\bar{\phi}(1/2, y) = \sin^2(2\pi y/L) \quad (78)$$

Numerical results on a 30×30 mesh are shown in Figure 26. There is little to differentiate between the $\bar{\phi}_h$ and ϕ_h in this case. Both representations are very accurate and there is no appearance of crosswind diffusion.

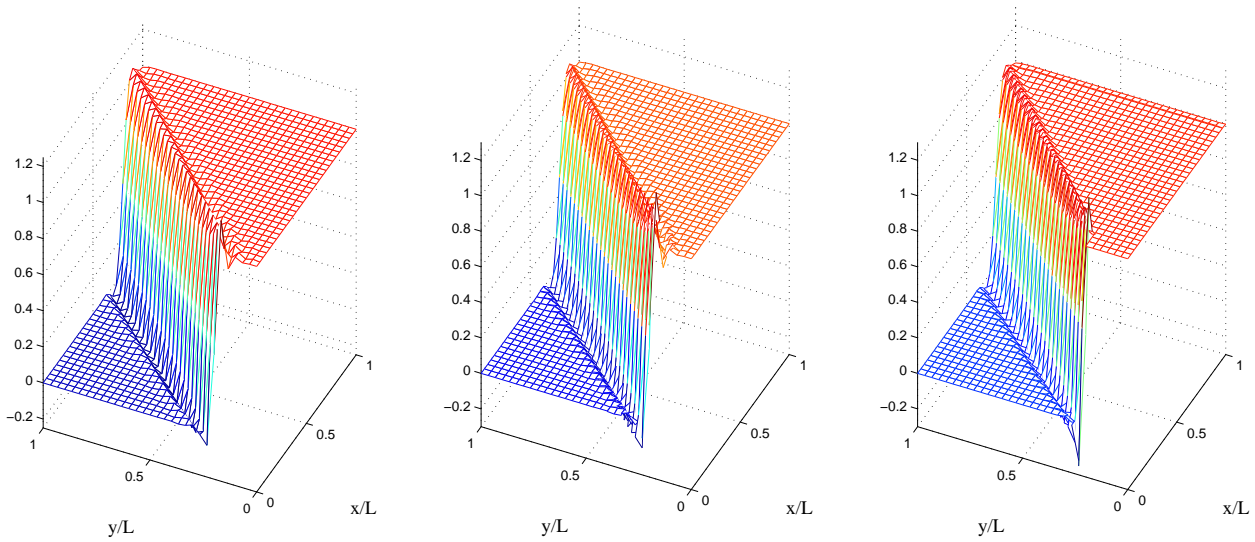


Figure 22: Advection skew to the mesh, $\theta = 45^\circ$. Left, continuous representation of the MDG solution, $\bar{\phi}_h$; center, discontinuous representation, ϕ_h ; right, solution of the global DG method without local condensation.

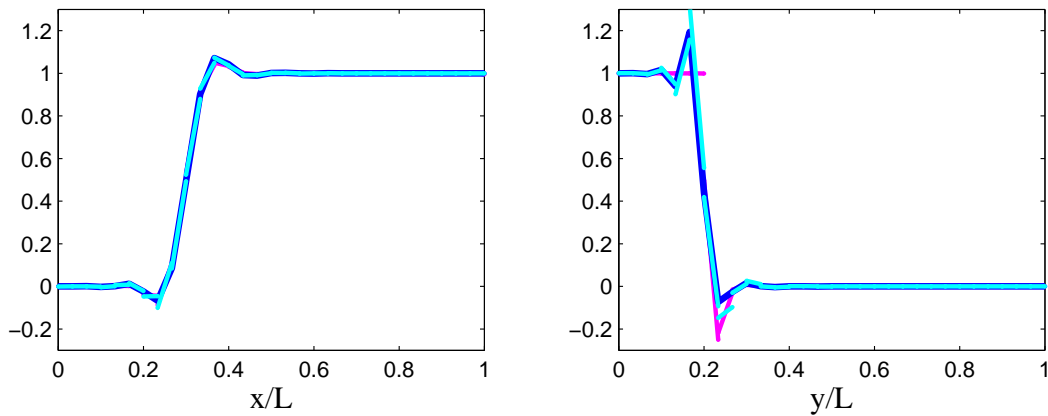


Figure 23: Advection skew to the mesh, $\theta = 45^\circ$. Left, solution at $y/L = .5$; right, solution at $x/L = 0$. Blue, MDG $\bar{\phi}_h$; light blue, MDG ϕ_h ; magenta, global DG solution without local condensation.

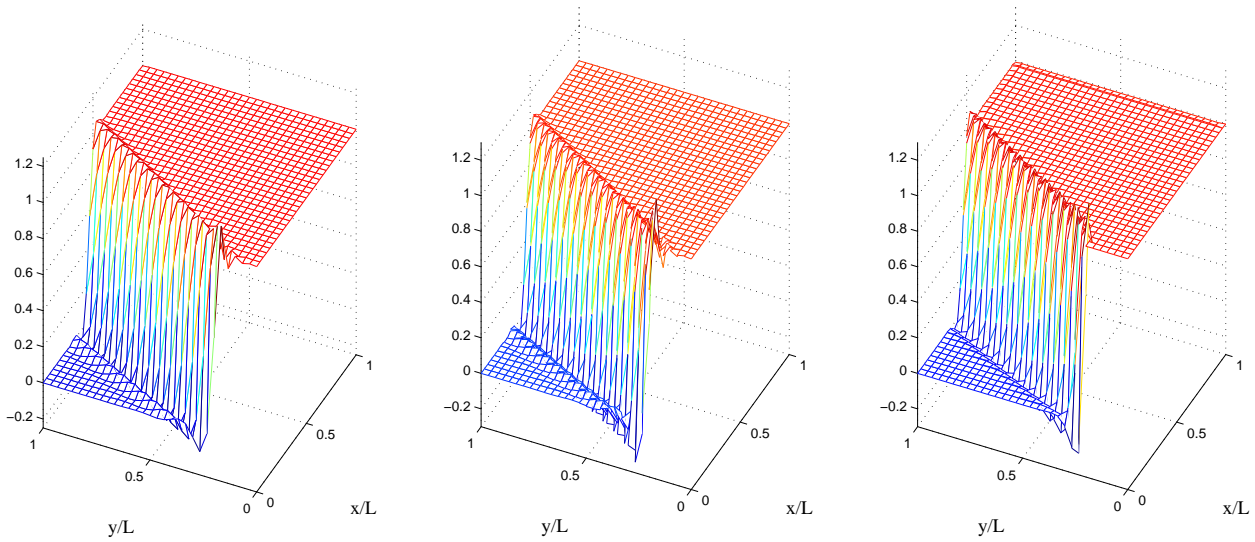


Figure 24: Advection skewed to the mesh, $\theta = 60^\circ$. Left, continuous representation of the MDG solution, $\bar{\phi}_h$; center, discontinuous representation, ϕ_h ; right, solution of the global DG method without local condensation.

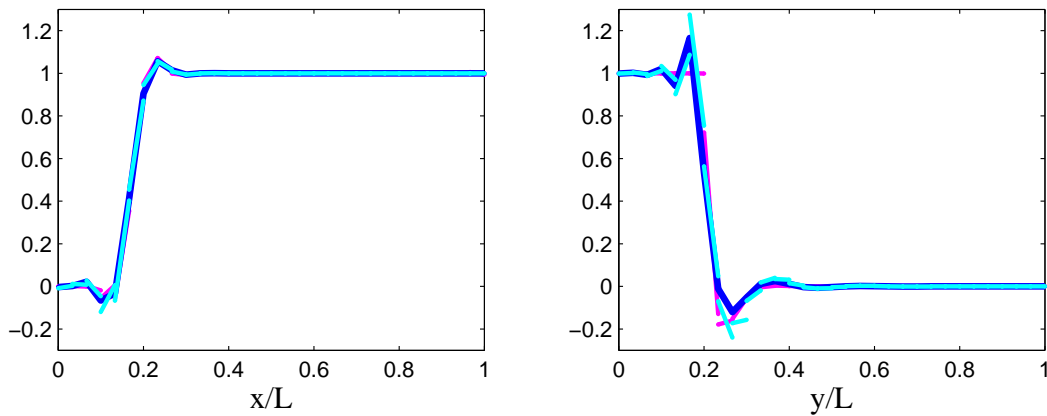


Figure 25: Advection skewed to the mesh, $\theta = 60^\circ$. Left, solution at $y/L = .5$; right, solution at $x/L = 0$. Blue, MDG $\bar{\phi}_h$; light blue, MDG ϕ_h ; magenta, global DG solution without local condensation.

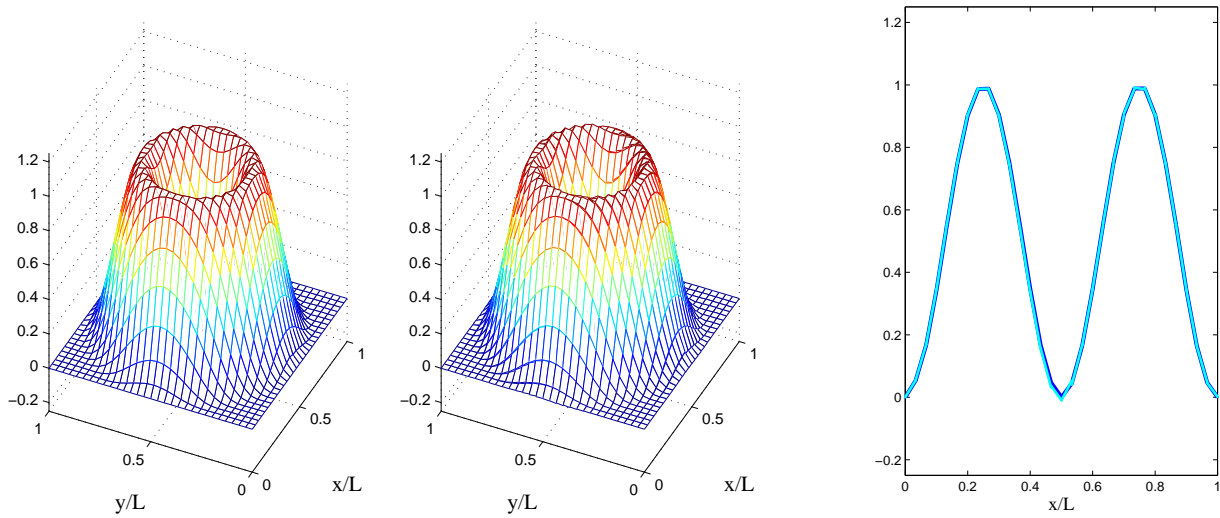


Figure 26: Rotating flow. Left, continuous representation of the MDG solution, $\bar{\phi}_h$; center, discontinuous representation ϕ_h ; right, solution at $y/L = .5$, in which the continuous and discontinuous solutions are seen to overlap.

6 Conclusions and Future Directions

The objective of the present work was to develop a discontinuous Galerkin method with the reduced computational cost of a corresponding continuous Galerkin method. The method developed achieves this objective and, at the same time, at least attains, and even somewhat improves upon, the performance of the associated continuous Galerkin method. This represents a solution to a fundamental and long-standing problem in discontinuous-Galerkin technology, namely, restraining the proliferation of degrees-of-freedom. Having accomplished this, there is still room for improvement. The discontinuous Galerkin method is certainly more robust than the continuous Galerkin method but, in itself, is not sufficiently robust for many industrial applications. Its improved stability exists primarily along characteristics but not perpendicular to characteristics. The “advection skew to the mesh” problem is illustrative of this fact. There are no oscillations present in the vicinity of the outflow Dirichlet boundary conditions but the internal layer gives rise to transverse oscillations. This deficiency is also present in SUPG (see Brooks and Hughes [10]), and it has long been recognized that additional mechanisms are necessary to produce sufficiently smooth solutions for industrial purposes. In the context of SUPG, this has motivated the development of “discontinuity capturing operators.” See Hughes, Mallet and Mizukami [36] and Hughes and Mallet [35] for the initial conceptions. Numerous improved variants have been developed subsequently by other researchers (see, e.g., [11, 19–22, 24, 26, 48]). Within the framework of the multiscale discontinuous Galerkin method, the local problem provides a vehicle for incorporating desired features. There seems to be a potential connection here with ideas from wave propagation methods based on solutions of the Riemann problem. This would appear to be a fruitful direction for further research, especially in the context of complex nonlinear problems. Other research challenges involve the mathematical basis of the multiscale discontinuous Galerkin method. Its structure is somewhat non-traditional in that solutions involve two distinct representations: the coarse-scale, continuous representation, $\bar{\phi}_h$, and the coarse-scale plus fine-scale discontinuous representation, $\phi_h = \bar{\phi}_h + \phi'_h$. In addition, the multiscale method requires stabilization terms to control the solution at outflow and sink nodes in the advection-dominated limit. This raises additional mathematical questions.

Acknowledgement

The authors would like to thank Giancarlo Sangalli for helpful remarks. The work of T. J. R. Hughes and G. Scovazzi was supported by Sandia Contract No. A0340.0 with the University of Texas at Austin. This support is gratefully acknowledged.

References

- [1] S. Adjerid, K. D. Devine, J. E. Flaherty, and L. Krivodonova. A posteriori error estimation for discontinuous Galerkin solutions of hyperbolic problems. *Computer Methods in Applied Mechanics and Engineering*, **191**(11-12):1097–1112, 2001.
- [2] J. Albery and C. Carstensen. Discontinuous Galerkin time discretization in elastoplasticity: motivation, numerical algorithms, and applications. *Computer Methods in Applied Mechanics and Engineering*, **191**(43):4949–4968, 2002.
- [3] D. N. Arnold, F. Brezzi, B. Cockburn, and L. D. Marini. Unified analysis of discontinuous

- Galerkin methods for elliptic problems. *SIAM Journal on Numerical Analysis*, **39**(5):1749–1779, 2002.
- [4] C. E. Baumann and J. T. Oden. A discontinuous hp finite element method for convection-diffusion problems. *Computer Methods in Applied Mechanics and Engineering*, **175**:311–341, 1999.
- [5] R. Becker, P. Hansbo, and M. G. Larson. Energy norm a posteriori error estimation for discontinuous Galerkin methods. *Computer Methods in Applied Mechanics and Engineering*, **192**(5-6):723–733, 2003.
- [6] F. Brezzi, L. P. Franca, T. J. R. Hughes, and A. Russo. $b = \int g$. *Computer Methods in Applied Mechanics and Engineering*, **145**:329–339, 1997.
- [7] F. Brezzi, G. Manzini, D. Marini, P. Pietra, and A. Russo. Discontinuous Galerkin approximations for elliptic problems. *Numerical Methods for Partial Differential Equations*, **16**(4):365–378, 2000.
- [8] F. Brezzi and L. D. Marini. A nonconforming element for the Reissner-Mindlin plate. *Computers and Structures*, **81**(8-11):515–522, 2003.
- [9] F. Brezzi and A. Russo. Choosing bubbles for advection-diffusion problems. *Mathematical Models and Methods in Applied Sciences*, **4**:571–587, 1994.
- [10] A. N. Brooks and T. J. R. Hughes. Streamline upwind/Petrov-Galerkin formulations for convection dominated flows with particular emphasis on the incompressible Navier-Stokes equations. *Computer Methods in Applied Mechanics and Engineering*, **32**:199–259, 1982.
- [11] E. Burman and A. Ern. A nonlinear diffusion and discrete maximum principle for stabilized Galerkin approximations of the convection-diffusion-reaction equation. *Computer Methods in Applied Mechanics and Engineering*, **191**(35):3833–3855, 2002.
- [12] P. Castillo. A superconvergence result for discontinuous Galerkin methods applied to elliptic problems. *Computer Methods in Applied Mechanics and Engineering*, **192**(41-42):4675–4685, 2003.
- [13] B. Cockburn, G. E. Karniadakis, and C.-W. Shu (eds.). *Discontinuous Galerkin Methods: Theory, Computation and Applications*. Lecture Notes in Computational Science and Engineering, 11. Springer-Verlag, 2000.
- [14] C. Dawson. The P^{k+1} - S^k local discontinuous Galerkin method for elliptic equations. *SIAM Journal on Numerical Analysis*, **40**(6):2151–2170, 2003.
- [15] C. Dawson and J. Proft. Discontinuous and coupled continuous/discontinuous Galerkin methods for the shallow water equations. *Computer Methods in Applied Mechanics and Engineering*, **191**(41-42):4721–4746, 2002.
- [16] C. Dawson and J. Proft. Space-time discontinuous Galerkin finite element method with dynamic grid motion for inviscid compressible flows:II. Efficient flux quadrature. *Computer Methods in Applied Mechanics and Engineering*, **191**(41-42):4747–4780, 2002.

- [17] C. Dawson and J. Proft. Coupled discontinuous and continuous Galerkin finite element methods for the depth-integrated shallow water equations. *Computer Methods in Applied Mechanics and Engineering*, **193**(3-5):289–318, 2003.
- [18] C. Dawson and J. Proft. Discontinuous/continuous Galerkin methods for coupling the primitive and wave continuity equations of shallow water. *Computer Methods in Applied Mechanics and Engineering*, **192**(47-48):5123–5145, 2003.
- [19] P. A. B. de Sampaio and A. L. G. A. Coutinho. A natural derivation of discontinuity capturing operator for convection-diffusion problems. *Computer Methods in Applied Mechanics and Engineering*, **190**(46-47):6291–6308, 2001.
- [20] E. G. D. do Carmo and G. B. Alvarez. A new stabilized finite element formulation for scalar convection-diffusion problems: the streamline and approximate upwind Petrov-Galerkin method. *Computer Methods in Applied Mechanics and Engineering*, **192**(31-32):3379–3396, 2003.
- [21] E. G. D. do Carmo and G. B. Alvarez. A new upwind function in stabilized finite element formulations, using linear and quadratic elements for scalar convection-diffusion problems. *Computer Methods in Applied Mechanics and Engineering*, **193**(23-26):2383–2402, 2004.
- [22] G. J. Dong, X. Y. Lu, and L. X. Zhuang. Discontinuity-capturing finite element computation of unsteady flow with adaptive unstructured mesh. *Acta Mechanica Sinica*, **20**(4):347–353, 2004.
- [23] G. Engel, K. Garikipati, T. J. R. Hughes, M. G. Larson, L. Mazzei, and R. L. Taylor. Continuous/discontinuous finite element approximations of fourth-order elliptic problems in structural and continuum mechanics with applications to thin beams and plates, and strain gradient elasticity. *Computer Methods in Applied Mechanics and Engineering*, **191**(34):3669–3750, 2002.
- [24] C. C. Fang and T. W. H. Sheu. Development of an adaptive discontinuity-capturing hyperbolic finite element model. *International Journal of Numerical Methods in Fluids*, **44**(9):957–973, 2004.
- [25] C. Farhat, I. Harari, and U. Hetmaniuk. A discontinuous Galerkin method with Lagrange multipliers for the solution of Helmholtz problems in the mid-frequency regime. *Computer Methods in Applied Mechanics and Engineering*, **192**(11-12):1389–1419, 2003.
- [26] A. C. Galeao, R. C. Almeida, and S. M. C. Malta. Finite element analysis of convection dominated reaction-diffusion problems. *Applied Numerical Mathematics*, **48**(2):205–222, 2004.
- [27] P. Hansbo and M. G. Larson. Coupling of continuous and discontinuous Galerkin methods for transport problems. *Computer Methods in Applied Mechanics and Engineering*, **191**(29-30):3213–3231, 2002.
- [28] P. Hansbo and M. G. Larson. Discontinuous Galerkin methods for incompressible and nearly incompressible elasticity by Nitsche’s method. *Computer Methods in Applied Mechanics and Engineering*, **191**(17-18):1895–1908, 2002.

- [29] P. Houston, I. Perugia, and D. Schötzau. Energy norm a posteriori error estimation for mixed discontinuous Galerkin approximations of the Maxwell operator. *Computer Methods in Applied Mechanics and Engineering*, **194**(2-5):499–510, 2005.
- [30] P. Houston, C. Schwab, and E. Süli. Discontinuous hp -finite element methods for advection-diffusion-reaction problems. *SIAM Journal on Numerical Analysis*, **39**(6):2133–2163, 2002.
- [31] T. J. R. Hughes. Multiscale phenomena: Green’s functions, the Dirichlet-to-Neumann formulation, subgrid-scale models, bubbles and the origin of stabilized methods. *Computer Methods in Applied Mechanics and Engineering*, **127**:387–401, 1995.
- [32] T. J. R. Hughes, G. Engel, L. Mazzei, and M. G. Larson. A comparison of discontinuous and continuous Galerkin methods based on error estimates, conservation, robustness and efficiency. In B. Cockburn, G.E. Karniadakis, and C.-W. Shu, editors, *Discontinuous Galerkin Methods: Theory, Computation and Applications*. Springer-Verlag, 2000.
- [33] T. J. R. Hughes, G. R. Feijóo, L. Mazzei, and J.-B. Quincy. The Variational Multiscale Method — a paradigm for computational mechanics. *Computer Methods in Applied Mechanics and Engineering*, **166**:3–24, 1998.
- [34] T. J. R. Hughes, L. P. Franca, and G. M. Hulbert. A new finite element formulation for computational fluid dynamics. VIII. The Galerkin/least-squares method for advective-diffusive equations. *Computer Methods in Applied Mechanics and Engineering*, **73**(2):173–189, 1989.
- [35] T. J. R. Hughes and M. Mallet. A new finite element method for computational fluid dynamics: III. The generalized streamline operator for multidimensional advection-diffusion systems. *Computer Methods in Applied Mechanics and Engineering*, **58**(3):305–328, 1986.
- [36] T. J. R. Hughes, M. Mallet, and Mizukami A. A new finite element method for computational fluid dynamics: II. Beyond SUPG. *Computer Methods in Applied Mechanics and Engineering*, **54**(3):341–355, 1986.
- [37] T. J. R. Hughes, A. Masud, and J. Wan. A stabilized mixed discontinuous Galerkin method for Darcy flow. *Computer Methods in Applied Mechanics and Engineering*, to appear.
- [38] T. J. R. Hughes and G. N. Wells. Conservation properties for the Galerkin and stabilized forms of the advection-diffusion and incompressible Navier-Stokes equations. *Computer Methods in Applied Mechanics and Engineering*, **194**:1141–1159, 2005.
- [39] T.J.R. Hughes, G. Engel, L. Mazzei, and M.G. Larson. The continuous Galerkin method is locally conservative. *Journal of Computational Physics*, **163**(2):467–488, 2000.
- [40] C. Johnson, U. Nävert, and J. Pitkäranta. Finite element methods for linear hyperbolic problems. *Computer Methods in Applied Mechanics and Engineering*, **45**:285–312, 1984.
- [41] C. Johnson and J. Pitkäranta. An analysis of the discontinuous Galerkin method for a scalar hyperbolic equation. *Mathematics of Computation*, **46**(173):1–26, 1986.
- [42] P. Lesaint and P. A. Raviart. On a finite element method for solving the neutron transport equation. In de Boor C., editor, *Mathematical Aspects of Finite Elements in Partial Differential Equations*. Academic Press, New York, 1974.

- [43] L. Machiels. A posteriori finite element bounds for output functionals of discontinuous Galerkin discretizations of parabolic problems. *Computer Methods in Applied Mechanics and Engineering*, **190**(26-27):3401–3411, 2001.
- [44] J. Palaniappan, R. B. Haber, and R. L. Jerrard. A spacetime discontinuous Galerkin method for scalar conservation laws. *Computer Methods in Applied Mechanics and Engineering*, **193**(33-35):3607–3631, 2004.
- [45] S.-H. Park and J. L. Tassoulas. A discontinuous Galerkin method for transient analysis of wave propagation in unbounded domains. *Computer Methods in Applied Mechanics and Engineering*, **191**(36):3983–4011, 2002.
- [46] W. H. Reed and T. R. Hill. Triangular mesh methods for the neutron transport equation. Technical report, LA-UR-73-479, Los Alamos Scientific Laboratory, 1973.
- [47] G. Sangalli. A discontinuous residual-free bubble method for advection-diffusion problems. *Journal of Engineering Mathematics*, **49**:149–162, 2004.
- [48] Y. T. Shih and H. C. Elman. Modified streamline diffusion schemes for convection-diffusion problems. *Computer Methods in Applied Mechanics and Engineering*, **174**(1-2):137–151, 1999.
- [49] G. N. Wells, K. Garikipati, and L. Molari. A discontinuous Galerkin formulation for a strain gradient-dependent damage model. *Computer Methods in Applied Mechanics and Engineering*, **193**(33-35):3633–3645, 2004.
- [50] T. Werder, K. Gerdes, D. Schötzau, and C. Schwab. *hp*-Discontinuous Galerkin time stepping for parabolic problems. *Computer Methods in Applied Mechanics and Engineering*, **190**(49-50):6685–6708, 2001.